Rapid Monitoring and Assessment of Drought in Papua New Guinea using Satellite Imagery

Final Report

to

United Nations Development Program
Port Moresby
Papua New Guinea

by

Phil N. Bierwirth[1] and Tim R. McVicar[2]
September 1998

1 Australian Geological Survey Organisation, PO Box 378, Canberra 2601, Australia.
2 CSIRO Land and Water, PO Box 1666, Canberra 2601, Australia.

Authors

Phil N. Bierwirth[1] and Tim R. McVicar[2]

1 Australian Geological Survey Organisation, PO Box 378, Canberra 2601, Australia.
pbierwir@agso.gov.au 61-2-6249-9231
2 CSIRO Land and Water, PO Box 1666, Canberra 2601, Australia.
tim.mcvicar@cbr.clw.csiro.au 61-2-6246-5741

ISBN

For bibliographic purposes, this document may be cited as:
Bierwirth, P. N. and McVicar, T. R. (1998) Rapid Monitoring and Assessment of Drought in Papua New Guinea using Satellite Imagery. Consultancy Report to United Nations Development Program, Port Moresby, Papua New Guinea, pp. 60.

For additional copies of this publication please contact:

Publication Enquires

CANBERRA
ACT 2601
AUSTRALIA

enquiries@

http://www

Executive Summary

Remotely sensed data from the Advanced Very High Resolution Radiometer (AVHRR) sensor was used to rapidly monitor and assess the 1997 drought experienced in Papua New Guinea (PNG). Data was purchased for a normal year (1996), the drought (1997) and for the year of recovery (1998). To overcome the problem of high amounts of cloud coverage experienced in the tropics, 4-week and 8-week composite data were used. The processing pathway developed in this project, which has been transferred to local scientists, is fully documented in this report. The Normalised Difference Vegetation Index (NDVI) and surface temperature (Ts) were both used. To utilise the negative correlation exhibited between these two variables the ratio of Ts/NDVI was plotted as a time series and mapped as time difference images. This provided a rapid indicator of drought, which does not require ancillary meteorological data.

Institutional Acronyms

ACRES	Australian Centre for REmote Sensing
AGSO	Australian Geological Survey Organisation
CSIRO	Commonwealth Scientific Industrial Research Organisation
DAL	Department of Agriculture and Livestock (PNG)
NASA	National Aeronautics and Space Administration (USA)
NOAA	National Oceanographic and Atmospheric Administration (USA)
PNGGS	Papua New Guinea Geological Survey
UNDP	United Nations Development Program

Scientific Acronyms

AE	Available Energy
AVHRR	Advanced Very High Radiometric Resolution
BIL	Band Interleaved by Line
BRDF	Bidirectional Reflectance Distribution Function
CWSI	Crop Water Stress Index
DEM	Digital Elevation Model
EMS	Electromagnetic Spectrum
ENSO	El Nino Southern Oscillation
ERS	Earth Resource Satellite
ET	Evapotranspiration
GAC	Global Area Coverage
GIS	Geographic Information System
GMS	Geostationary Meteorological Satellite
JERS	Japanese Earth Resources Satellite
LAC	Local Area Coverage
LAI	Leaf Area Index
MODIS	MODerate-resolution Imaging Spectroradiometer
MSS	Multi-Spectral Sensor
NDTI	Normalised Difference Temperature Index
NDVI	Normalised Difference Vegetation Index
NIR	Near InfraRed
RADAR	RAdio Detection And Ranging
SAR	Synthetic Aperture RADAR
SEB	Surface Energy Balance
SOI	Southern Oscillation Index
TM	Thematic Mapper
Ts	Surface Temperature
VISSR	Visible and Infrared Spin Scan Radiometer
VITT	Vegetation Index Temperature Trapezoid

1.0 Introduction

This report demonstrates how hi-frequency remote sensing has been used to monitor and assess the 1997 drought in Papua New Guinea (PNG). This project was funded by the United Nations Development Program (UNDP). The funds allowed for suitable satellite imagery to be acquired, and for a short visit (2 weeks) by the two authors of this report to PNG. This report documents the establishment of the remote sensing data base, the technology transfer and the data analysis that was undertaken during the course of this project.

The stated aims of this project are to:

1. determine if hi-frequency remotely sensed data allows drought conditions in PNG to be monitored;
2. transfer the technology, if monitoring of drought is possible, so that Officials from several PNG National Government Departments have the ability to undertake the analysis of hi-frequency remote sensing data;
3. provide assistance with the scientific interpretation of the remotely sensed data of the drought experienced by PNG in 1997; and
4. provide recommendations, based on the findings of 2 and 3 above, on operational systems that could be established, using readily available data to assist PNG in monitoring and assessing the 1997 drought. Consideration is given to developing an early warning of future drought situations. The monitoring of actual, rather than potential conditions, is still considered important.

In undertaking this project visits were made to organisations that had first hand experience in dealing with the assessment and response to the 1997 drought. These included the:

- Papua New Guinea Geological Survey (PNGGS)
- Papua New Guinea Department of Agriculture and Livestock (DAL)
- Papua New Guinea Meteorological Office
- Australian National University, Department of Human Geography
- Australian National University, Centre for Resources and Environmental Studies

For a comprehensive listing of individuals contacted during this project, refer to Appendix 1. An introduction to PNG and the drought of 1997 is given in the following section. A background to remote sensing is provided in Section 3. Specialists in any of these areas need not wade through this material; they provide full context.

2.0 Papua New Guinea and the 1997 Drought

Papua New Guinea is comprised of the eastern half of the island of New Guinea and the archipelago extending to the East of the main island. The western portion of the island of New Guinea is Irian Jaya, Indonesia. PNG extends from the equator to 12 degrees South and longitudes 141 to 156 degrees East. The total land area is over 460,000 km^2. The main island of PNG is 1,100 km east-west and 900 km north-south, see Fig. 1.

Drought is a complex natural event. A universally accepted definition of drought does not exist (Wilhite, 1993). It is acknowledged that the major cause of drought is lower than average rainfall. The rainfall deficit will have different impacts depending on other factors including, meteorological conditions, ecosystem type, and social and economic circumstances. Currently, there are four major types of drought which are broadly defined and agreed upon in the scientific literature (WMO, 1975, Wilhite and Glantz, 1985, White, 1990, Alley, 1984, Alley, 1985). These are:

1. *meteorological drought*, which is generally regarded as being lower than average precipitation for some time period. In some cases air temperature and precipitation anomalies may be combined;
2. *agricultural drought*, occurs when plant available water, from precipitation and water stored in the soil, falls below that required by a plant community during a critical growth stage. This leads to below average yields in both pastoral and crop producing regions;
3. *hydrologic drought* is generally defined by one or a combination of factors such as stream flow, reservoir storage and groundwater; and
4. *socioeconomic drought* is defined in terms of loss from an average or expected return. It can be measured by both social and economic indicators, of which profit is only one.

We consider drought to be a period when lower than average rainfall was received and agricultural production systems fell below capacity. This definition is a hybrid between the classic meteorological and agricultural drought definitions. In this study we are looking for broad indicators of drought from hi-frequency remotely sensed data; we are not attempting to use this data to define and map drought conditions for legislative measures.

Drought conditions in PNG may be defined as occurring when rainfall was lower than average for periods greater than 10 weeks (Bourke *pers. comm*.). There is a long and well documented history of drought events occurring in PNG, often associated with El Nino events (Nicholls, 1973, Allen, 1989, Allen *et al.*, 1989). In PNG drought conditions affect the food supply to the subsistence based agricultural communities in two ways: (I) decrease of plant available water; and (II) frost occurrence in the highlands. The lack of rainfall decreases the plant available water, which in turn may result in reduction of plant cover. This affects the production of food relied upon by the subsistence agricultural communities. This reduction in plant cover is one parameter that is observed using remotely sensed data, see section 3.1. During dry conditions more incoming short-wave radiation reaches the ground (due to there being less cloud cover) and more of this is partitioned into the sensible heat flux (rather than the latent heat flux), resulting in higher land surface temperatures, see section 3.2. The response of land surface temperatures (an increase) is slight faster than the response of plant cover (a decrease) due to reduced moisture availability associated with drought conditions.

Within the PNG highlands there is a belt of dense human habitation between the altitudes of 1 400m to 2 850m above sea level (Brookfield and Allen, 1989). Drought conditions are associated with low amounts of cloud cover. Due to the cloudless nights and the consequent loss of long-wave radiation, surface cooling results in frosts. The highland agricultural systems are subsistence-based; relying heavily on the frost intolerant sweet potato. If frost is experienced prior to tuber bulking the crop may be delayed by several months, however, if frost occurs during or after the bulking phase the subsequent tubers are inedible (Bourke, 1989). Recently some frost tolerant crops have been introduced.

During the 1997 drought, low plant water availability and frosts were experienced (Bourke, 1998, Allen *et al.*, 1997, Allen and Bourke, 1997, Allen, 1998). This meant that populations relying on subsistence-based agriculture needed supplementary food supplies. Some 1.2 million rural villagers suffered a severe, and in some cases fatal, food shortage during the 1997 drought event in PNG. This is almost 40 percent of the rural population (Allen and Bourke, 1997, Allen, 1998). The 1997 event is considered to the the "drought of the century" (Bourke, 1998), the associated food and water shortages strained emergency services beyond their limits (Bourke, 1998, Allen, 1998). The onset of drought can cause both immediate food shortages (due to frosts) and longer term food shortages (due to decreased plant water availability). Both the onset of drought conditions and the recovery from drought are important factors in a drought event; both phases are considered in this report.

The percent divergence from monthly average rainfall, shown in Fig. 2, reveals that many stations during 1997 received below average rainfall for several months. Large areas of PNG have no reliable meteorological ground recording facilities (Fig. 2). Some of these areas are sparsely populated. However, the number of ground based stations has been decreasing over the last 20 years. A characteristic of remote sensing is its synoptic coverage which provides vast opportunities for monitoring the 1997 drought event in PNG.

3.0 Background of Remote Sensing

Remote sensing is the acquisition of digital data in the gamma, reflective, thermal or microwave portions of the electromagnetic spectrum (EMS). Fig. 3 is a schematic diagram of electromagnetic radiation. Measurements of the EMS are be made either from satellite, aircraft or ground-based systems, but it is characteristically at a distance (or "remote") from the target. Due to the large spatial extent of PNG, this paper will focus on data gathered from satellite remote sensing systems.

Remotely sensed images are recorded digitally by sensors on board the satellites. A schematic of satellite based remote sensing is shown in Fig. 4. The resulting images can be manipulated by computers to highlight features of soils, vegetation and clouds. Each pixel, or picture element, contributing to the image is a measurement of a particular wavelength of electromagnetic radiation at a particular spatial scale for a particular location at a specific time. The most common display of remotely sensed data is a single overpass, which non-remote sensing specialists may think of as a 'satellite photo'.

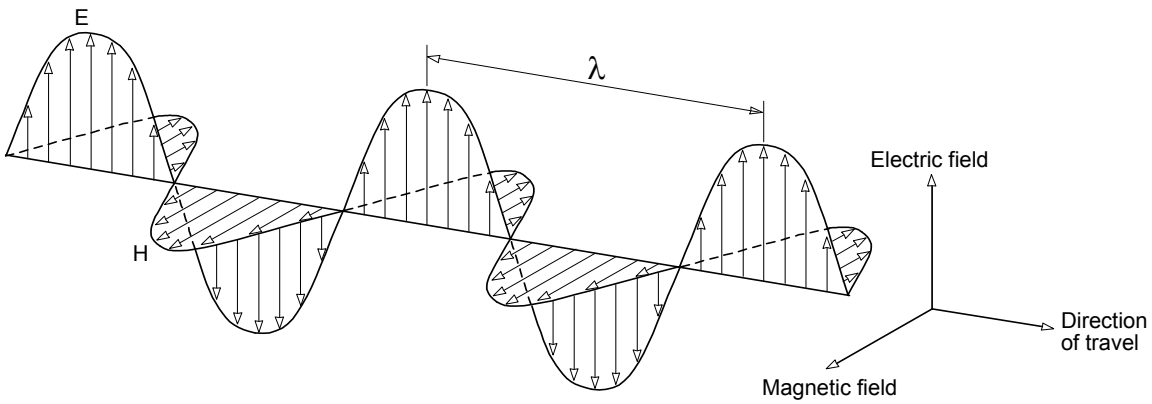

Fig. 3: An electromagnetic wave comprises two sinusoidal waves: an electric and a magnetic wave. Wavelength (λ) is the distance between successive wave peaks. Adapted from (Harrison and Jupp, 1989).

Remotely sensed data are spatially dense. This means that for the extent of the image it is a census at a particular spatial scale and electromagnetic wavelength. It is not a point sample. There may be distances of 200 kilometers between meteorological stations, or field sites. Remotely sensed data are measurements at, say, 1 km spatial resolution for each and every one of the 200 km separating the stations.

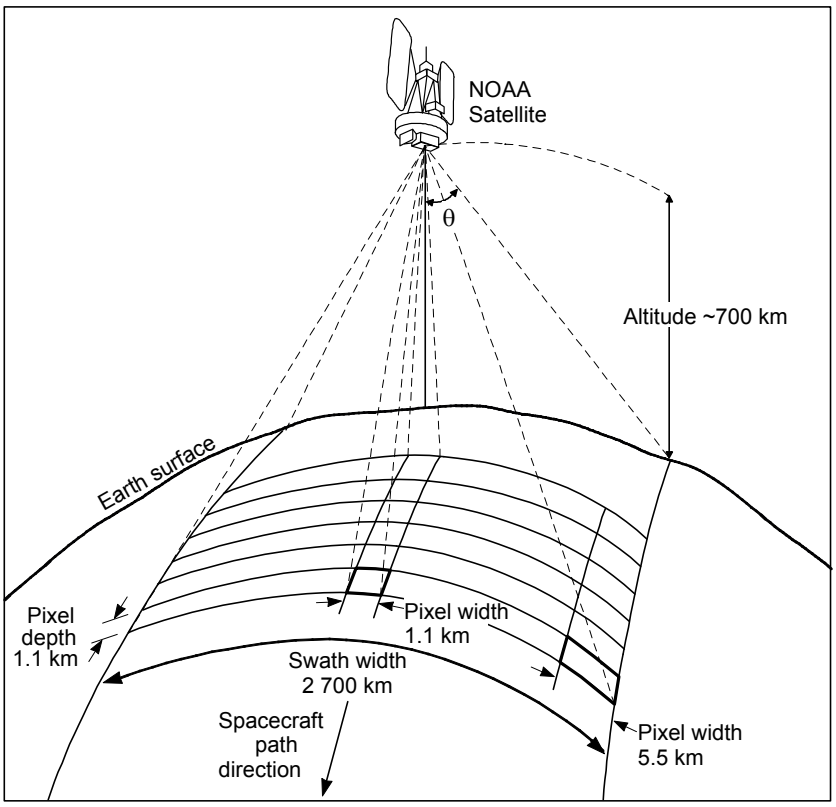

Fig. 4: Schematic of satellite operation. The data acquisition of the Advanced Very High Resolution Radiometer (AVHRR) sensor operates onboard the United State Federal Agency National Oceanographic and Atmospheric Administration (NOAA) series of satellites. Adapted from (Harrison and Jupp, 1989).

When dealing with remotely sensed images, the extent, resolution (or integration) and density of the spectral, spatial and temporal characteristics need to be kept in mind. Information for current reflective and thermal satellite remote sensing systems is presented in Table 1 and for current RADAR satellite based systems in Table 2.

Spectral:

- Spectral extent describes what portion of the electromagnetic spectrum is being sampled, for example, is it just visible or does the range extend into the thermal.
- Spectral resolution refers to the bandwidths of each channel.
- Spectral density indicates the number of band in a particular portion of the EMS, for example hyperspectral sensors have higher spectral density than broadband instruments.

Spatial:

- Spatial extent is the area covered by the image.
- Spatial resolution refers to the smallest pixel or picture element acquired.
- Spatial density is complete, compare this with the spatial density of rainfall stations in the example above.

Temporal:

- Temporal extent is the recording period over which the data is available, for some systems data has been recorded for 25 years.
- Temporal resolution is the time that the data is acquired over, usually this is a matter of seconds, compare this to the daily rainfall totals.
- Temporal density is the repeat characteristics of the satellite and for some applications the availability of cloud free data.

The extent, resolution and density of remotely sensed data and other data sources, such as ground based meteorological data, needs to be understood to be used in drought mapping and monitoring systems.

Remote sensing of the land surface occurs at wavelengths of the EMS where the light can pass through the Earth's atmosphere with no, or little, interaction with the atmosphere. These bands of the EMS are called 'atmospheric windows' and refer to the spectral extent in which radiation reaching remote sensing instruments carries information about the Earth's surface conditions. These 'atmospheric windows' are defined by the transmittance of the constituents of the Earth's atmosphere. There are some gases which absorb all electromagnetic radiation in certain wavelengths preventing these areas of the EMS being used for remote sensing. The electromagnetic spectrum is divided into regions (Fig. 5).

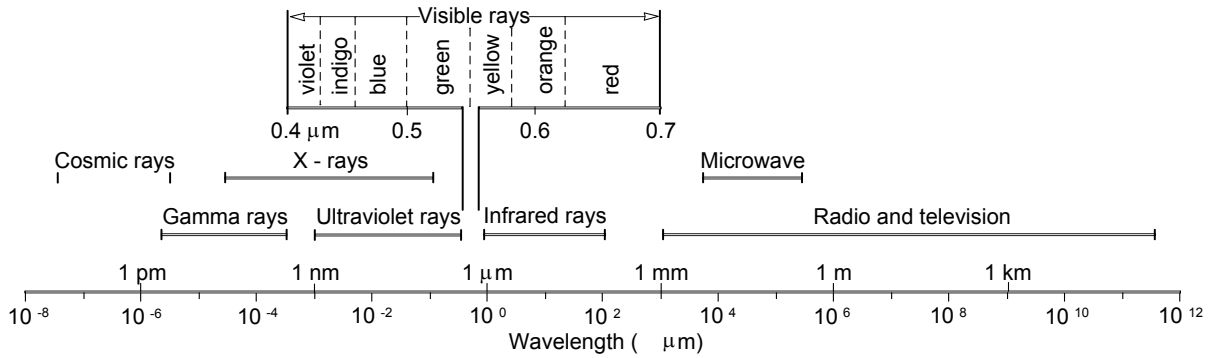

Fig. 5 The electromagnetic spectrum is divided into regions for convenience, there are no clear divisions. Note that the scale is logarithmic. Adapted from (Harrison and Jupp, 1989).

3.1 Reflective Remote Sensing

The reflective portion of the EMS ranges nominally from 0.4 to 3.75 micro meters (μm). Light of shorter wavelength than this is termed ultraviolet (Fig. 5). The reflective portion of the EMS can be further subdivided into the visible 0.4 to 0.7 μm, near infrared (NIR) 0.7 to 1.1 μm, and mid infrared 1.1 to 3.75 μm. It is in the visible portion of the EMS that we

sense with our remote sensing device (eyes) which allow us to see. Different surface reflective properties allow us to distinguish colour in the visible region of the EMS.

Chlorophyll pigments that are present in leaves absorb red light. In the NIR portion, radiation is scattered by the internal spongy mesophyll leaf structure which leads to higher values in the NIR channels. This interaction between leaves and the light that strikes them is one determinant of the different responses in the red and NIR portions of reflective light (Fig. 6). Most vegetation indices are combinations of these two reflective bands. The most common linear combinations are the simple ratio (NIR/Red) and Normalised Difference Vegetation Index (NDVI) = (NIR-Red)/(NIR+Red). Previous research has shown positive correlations exist between foliage presence, including measurements of LAI (Tucker, 1979), and plant condition (Sellers, 1985), and vegetation indices such as the simple ratio and NDVI. For a comprehensive listing of vegetation indices refer to Tian (1989), Kaufman and Tanre (1992), Thenkabail *et al.* (1994) and Leprieur *et al*. (1996).

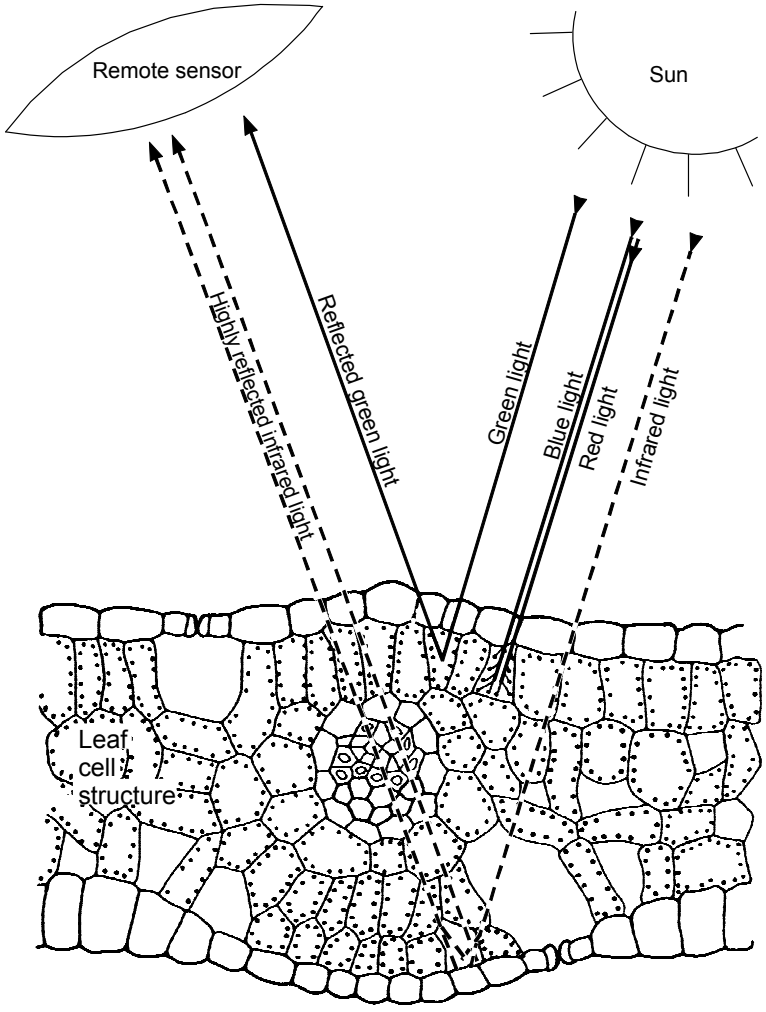

Fig. 6: Schematic reflectance of a typical green leaf in cross section. The chloroplasts reflect the green light absorb the red and blue wavelength for use on photosynthesis. The near infrared light is highly scattered by water in the spongy mesophyll cells. Adapted from (Harrison and Jupp, 1989).

While the amount of leaf is one determinant of the signal strength in the reflective portion of the EMS there are several other important factors which control the acquired value. These include the sun-target-sensor geometry. This will control the amount of shadow contributing to the signal; the shadow may be driven by insolation effects due to regional topography and may also be influenced by vegetation shadowing. This effect, termed the bidirectional reflectance distribution function (BRDF) (Burgess and Pairman, 1997, Deering, 1989), is characteristic of vegetation structure. Other effects in the reflective portion of the EMS include changes in soil colour and changes in the observed signal due to changes in the atmospheric component of the signal, including atmospheric precipitable water (Choudhury and DiGirolamo, 1995, Hobbs, 1997), and changes in the response of the sensor over time.

The uses of the reflective portion of the EMS for drought assessment and monitoring are reviewed by McVicar and Jupp (1998).

3.2 Thermal Remote Sensing

The thermal portion of the EMS ranges nominally from 3.75 to 12.5 micro meters (Fig. 5). The radiant energy observed by sensors is emitted by the surface, be it land, ocean or cloud top, and is a function of surface temperature. Models have been developed to allow surface temperature to be extracted from thermal remote sensing. Prata (1994) and Prata *et al*. (1995) review the algorithms and issues involved in the calculation of land surface temperatures.

Thermal remote sensing is an instantaneous observation of surface temperature which in turn is related to the status of the surface energy balance (SEB). The SEB is driven by the net radiation at the surface. During the daytime this is usually dominated by incoming short-wave radiation from the sun, the amount reflected depending on the albedo of the surface. There are also up and down welling long-wave components. At the ground surface the net allwave radiation is balanced between the sensible, latent and ground heat fluxes. Over long periods of time the ground heat flux averages out, and the SEB represents the balance with the sensible and latent heat fluxes. During the day the measured surface temperature at the Earth's surface is, in part, dependent on the relative magnitude of the sensible and latent heat fluxes.

The surface energy balance at any instant is given by:

$$R_n = \lambda E + H + G$$

where:
R_n is net all wavelength radiation (Wm^{-2});
E is the evapotranspiration (ET) flux ($m\ sec^{-1}$) of water vapor;
λ is latent heat of vaporisation of water ($J\ m^{-3}$);
H is sensible heat flux ($W\ m^{-2}$), or the energy involved in the movement of the air and its transfer to other objects (such as trees, grass etc); and
G is the ground heat flux into the soil or other storages ($W\ m^{-2}$).

λE denotes the amount of energy needed to change a certain volume of water from liquid to vapor, either by transpiration or evaporation. The combination of these two fluxes is called

evapotranspiration. The net available energy (AE) at the Earth's surface, which is available for conversion to other forms, can be written as

$$AE = R_n - G = \lambda E + H$$

where the terms are defined as above. A key factor determining the observed surface temperature is the partitioning of the AE into the latent and sensible heat fluxes. This is governed by the amount of water available and the ease with which it is transferred from the surface to the atmosphere, via ET. For given meteorological conditions there will also be a potential ET which could occur if water was not limiting. The ratio of the actual to potential ET is termed the moisture availability.

Thermal remotely sensed data can also be recorded at night. During the night, the SEB is dominated by the release of heat from the ground, which was absorbed during the daylight hours. The release of heat during the night is governed by how much was absorbed during the day and the rate at which it is released after sunset. This is a function of the environment's capacity to store heat, which also depends on the amount of water stored in the environment.

The uses of the thermal portion of the EMS for drought assessment and monitoring are also reviewed by McVicar and Jupp (1998).

Table 1. General description of current satellite sensors which acquire reflective and / or thermal data which are useful for monitoring all of PNG for drought.

Satellite: Sensor	Channel #	Spectral Resolution	Spatial Resolution (m) at nadir	Sample Swath	Repeat Cycle	Lifetime
GMS:VISSR[1]	1	500-750 nm	1250	hemisphere	Hourly	1978 - present
	2	10.5-12.5 μm	5000			
NOAA:AVHRR[2]	1	580-680 nm	1100	2700 km	Every 12 hours	1981 - present
	2	725-1100 nm	"			
	3	3.55-3.93 μm	"			
	4	10.5-11.3 μm	"			
	5	11.5-12.5 μm	"			
LANDSAT:MSS[3]	4	500-600 nm	80	185 km	Every 16 days	1972 - present
	5	600-700 nm	"			
	6	700-800 nm	"			
	7	800-1100 nm	"			
LANDSAT:TM[4]	1	450-520 nm	30	185 km	Every 16 days	1983 - present
	2	520-600 nm	"			
	3	630-690 nm	"			
	4	769-900 nm	"			
	5	1.55-1.75 μm	"			
	7	2.08-2.35 μm	"			
	6	10.4-12.5 μm	120			

1 GMS:VISSR is the Geostationary Meteorological Satellite (GMS) launched by Japan provides images for Australasia. It is located above the equator at 140^0E at an altitude of some 36 000 km. The Visible and Infrared Spin Scan Radiometer (VISSR) is the main sensor used for meteorological remote sensing. In other parts of the globe similar data are available (Petty, 1995). The U.S. Geostationary Operational Satellite (GOES) series has a spatial resolution at nadir similar to the VISSR. The European Meteosat, which carries the Meteosat radiometer, has a spatial resolution at nadir of 2.5 km for the visible channel and 5 km for the thermal IR. The Indian INSAT carries the VHRR radiometer which a spatial resolution at nadir of 2.75 km for the visible channel and 11 km for the thermal IR.

2 NOAA:AVHRR refers to a series of satellites operated by the United State Federal Agency, NOAA, National Oceanographic and Atmospheric Administration. The Advanced Very High Resolution Radiometer (AVHRR) sensor operates on this platform. From 1978 to 1981 only the first 4 channels were acquired. The NOAA series of satellites are polar orbiting at a height of some 700 km, similar to the height of the LANDSAT series of satellites. AVHRR data are acquired over a large swath width, compared to the LANDSAT data, due to the wide scan angle, $\pm$ 55^o, of the AVHRR sensor. The Local Area Coverage (LAC) pixel size is 1100 m at the sub-satellite point, becoming 5400 m at the of edge of the swath. Global Area Coverage (GAC) data are also recorded by the AVHRR sensor. GAC is a sub-sampling of the LAC data and nominally has a 5 by 3 kilometer resolution. GAC data are recorded on board the satellite and recorded at the NASA Goddard Space Flight Centre.

Soon AVHRR data will be superseded Moderate-Resolution Imaging Spectroradiometer (MODIS) data. This is planned for launch in 1998 aboard EOS AM-1 and is the key instrument in NASA's Earth Observing System (EOS). A fleet of satellites is to be launched over the next two decades. MODIS is anticipated to continue and enhance the high temporal frequency coverage of remotely sensed data offered by the AVHRR sensor. MODIS has 36 bands with differing spatial resolutions (2 are 250m, 5 are 500m and the remaining 29 are 1 km) details of the increased spectral resolution of the bands can be found at the following WWW address: http://modarch.gsfc.nasa.gov/MODIS/MODIS.html

3 LANDSAT:MSS refers to the multispectral sensor (MSS) on board the LANDSAT series of satellites. From 1972 to 1983, for LANDSAT 1 - 3 the repeat cycle was 18 days. LANDSAT is a polar orbiting sun synchronous satellite, which passes a given latitude at the same solar time, it operates at a height of 700 km.

4 LANDSAT:TM refers to the thematic mapper (TM) sensor on board LANDSAT 4 and 5. Channels and wavelengths are not ascending due to the late inclusion of channel 7.

3.3 Microwave Remote Sensing

The microwave portion of the EMS ranges nominally from 0.75 to 100 centimeters (Fig. 5). Radio signals have wavelengths which are included in these bands. These systems can either be active (the sensor sends its own signal) or passive (the background signal from the Earth's surface is observed). There are five smaller sections of this range which are used for remote sensing. These are :

P band	100 - 30 cm;
L band	30 - 15 cm;

S band 15 - 7.5 cm;
C band 7.5 - 3.75 cm; and
X band 3.75 - 2.4 cm.

Both passive and active microwave observations have been related to near surface soil moisture for a number of experimental field sites. RADAR (RAdio Detection And Ranging), is an active system based upon sending a pulse of microwave energy and then recording the strength, and sometimes polarization, of the return pulses. The way the signal is returned provides information to determine characteristics of the landscape. RADAR has been used in the determination of near surface soil moisture. Technical specifications for current satellite RADAR systems are listed in Table 2.

Table 2. Technical specifications of current satellite based RADAR systems.

Sensor	Wavelength	Pixel Size (m^2)	Incidence Angle	Polarization	Swath Width (km)	Date recorded since	Current Repeat Cycle
JERS[1]	L-band	18	35°	HH	75	June 1993	44 days
ERS[2]	C-band	12.5	23°	VV	102.5	Sept 1991	35 days
RADARSAT[3]	C-band	100	20-49°	HH	500	Nov 1995	3 days

[1] JERS is the Japanese Earth Resources Satellite-1. It observes the Earth's surface using 8 spectral bands in the reflective portion of the EMS and the L-band synthetic aperture RADAR (SAR).

[2] ERS is the Earth Resource Satellite launched and operated by the European Space Agency. The SAR operates in the C-band.

[3] RADARSAT is a Synthetic Aperture RADAR on board a Canadian Satellite. The Scansar Wide mode is reported here, as it has the largest swath width and therefore has the most potential for PNG drought applications. The large incidence angle means that the repeat cycle is only a few days. However, the entire 30 degree range may not be suitable for the accurate estimation of soil moisture. ACRES offer a RADARSAT Scansar narrow mosaic for all PNG, made of 11 scenes. This is not time series data. RADARSAT data is recorded on demand by ACRES and a limited data archive exists for PNG. However, images can be ordered and acquired for any portion of PNG from ACRES.

To date only few studies have used satellite RADAR data to estimate soil moisture. Cognard *et al*. (1995) used data from ERS-1 to estimate soil moisture for a small catchment in France. Results show that stratifying vegetation cover into different classes provided a more reliable relationship. However, the most promising relationship was for cereals, for which ERS-1 data explained 20% of the variance observed in soil moisture over the study period. Reasons for this low predictive capability is that soil roughness and vegetation density as well as soil moisture, determine the observed RADAR signal. This is in part due to the unfavorable incidence angle of ERS-1 (Cognard *et al.*, 1995). It appears that RADAR data needs to be multi-frequency and multi-polarized to allow the interactions of soil roughness, vegetation density and soil moisture to be solved simultaneously. Currently, RADAR data with these characteristics is only available from special missions using the NASA aircraft based synthetic aperture RADAR system, AIRSAR.

McVicar and Jupp (1998) concluded that current satellite borne RADAR provided little operational potential for use in drought monitoring and assessment in Australia. Similar problems will exist in PNG. The reasons for this are:

1. L-band data penetrates the soil to a greater depth and is only available on JERS;
2. the JERS instrument has a small swath width and large repeat cycle which precludes monitoring all of PNG every month;
3. fixed incidence significantly limits the use of satellite based RADAR systems for the determination of soil moisture.

4.0 Methods

4.1 Selection of Remotely Sensed Data to Assess the PNG Drought

To rapidly assess and monitor the drought situation for all of PNG, it was decided to use AVHRR data. AVHRR data offers two main advantages: a frequent repeat cycle (so there are more opportunities to obtain cloud free imagery), and a complete coverage of PNG allowing drought conditions to be monitored (Table 1). The large spatial extent of PNG precluded using RADAR images as several images would need to be mosaiced to cover the entire country (Table 2). This data source was deemed to be too expensive, both in purchase costs (to develop a suitable time series with the appropriate spatial extent and repeat characteristics), and in terms of processing requirements. In addition to suffering the same problems as RADAR data, LANDSAT TM also suffers from the additional problem of cloud cover. This means that developing a suitable time series of LANDSAT TM imagery with the appropriate spatial extent and repeat characteristics was not possible (Table 1). Data from GMS covers the entire country; however there is only one reflective band and one thermal band. The varying pixel sizes also presents problems for drought analysis (Table 1).

To overcome the problems of cloud contaminated pixels, some AVHRR receiving stations process the images by compositing several AVHRR images together. The aim of the compositing procedure is to remove cloud effects (either pixels observing cloud or in cloud shadow) from the images. Cloud affected pixels and those with large off nadir viewing angles have depressed NDVI values. To avoid using these pixels in the composite image, data with the maximum NDVI are selected from a time period (*e.g.* fortnightly) of AVHRR images and used in the resultant composite image. Using the maximum NDVI means that data with poor atmospheric conditions and those that have large off nadir acquisition angles are not selected for the compositing procedure. Using linear band combination such as the NDVI also reduces some of the BRDF and other angular effects in the resulting images, however some residual noise may be still present after normalisation.

4.2 Establishing the AVHRR Time Series

Composite AVHRR data was purchased from CSIRO Marine Research based in Hobart, Australia. The original LAC data covering PNG was recorded at the Australian Centre for Remote Sensing (ACRES) satellite receiving station located at Alice Springs. The data from Alice Springs is sent to Hobart where compositing algorithms are applied to the data. For this project CSIRO Marine Research developed suitable compositing algorithms to cover PNG. Data from this process is available from CSIRO Marine Reseach in Hobart by using the WWW, an example of this is provided in Section 5.2.

Both 2-week and 4-week composite images starting in January 1996 were purchased from CSIRO Marine Research in Hobart. The project has funds available to continue to purchase imagery until the end of 1998, through the recovery phase of the drought event. The start date and end date of the 2 week composite period is listed in Table 3. The system developed and transferred to local agencies during this project is called PNG Drought AVHRR Time Series, which is shortened to PNG_DATS in this report.

Table 3. Lists the 2-week AVHRR composites from CSIRO Marine Research, Hobart. The date code has the format YYYYMMDD, where YYYY is the year, MM is the month, and DD is the date. The Hobart Mosaic Number is a relevant to the processing stream data documentation internal to CSIRO Marine Research, Hobart and is listed to ensure complete data flow documentation.

Hobart Mosaic #	Start Date	End Date	Hobart Mosaic #	Start Date	End Date
129	19951230	19960112	169	19970712	19970725
130	19960113	19960126	170	19970726	19970808
131	19960127	19960209	171	19970809	19970822
132	19960210	19960223	172	19970823	19970905
133	19960224	19960308	173	19970906	19970919
134	19960309	19960322	174	19970920	19971003
135	19960323	19960405	175	19971004	19971017
136	19960406	19960419	176	19971018	19971031
137	19960420	19960503	177	19971101	19971114
138	19960504	19960517	178	19971115	19971128
139	19960518	19960531	179	19971129	19971212
140	19960601	19960614	180	19971213	19971226
141	19960615	19960628	181	19971227	19980109
142	19960629	19960712	182	19980110	19980123
143	19960713	19960726	183	19980124	19980206
144	19960727	19960809	184	19980207	19980220
145	19960810	19960823	185	19980221	19980306
146	19960824	19960906	186	19980307	19980320
147	19960907	19960920	187	19980321	19980403
148	19960921	19961004	188	19980404	19980417
149	19961005	19961018	189	19980418	19980501
150	19961019	19961101	190	19980502	19980515
151	19961102	19961115	191	19980516	19980529
152	19961116	19961129	192	19980530	19980612
153	19961130	19961213	193	19980613	19980626
154	19961214	19961227	194	19980627	19980710
155	19961228	19970110	195	19980711	19980724
156	19970111	19970124	196	19980725	19980807
157	19970125	19970207	197	19980808	19980821
158	19970208	19970221	198	19980822	19980904
159	19970222	19970307	199	19980905	19980918
160	19970308	19970321	200	19980919	19981002
161	19970322	19970404	201	19981003	19981016
162	19970405	19970418	202	19981017	19981030
163	19970419	19970502	203	19981031	19981113
164	19970503	19970516	204	19981114	19981127
165	19970517	19970530	205	19981128	19981211
166	19970531	19970613	206	19981212	19981225
167	19970614	19970627	207	19981226	19990108
168	19970628	19970711			

Two 2-week AVHRR composites have been merged, based on the maximum NDVI into a 4-week composite, the period is listed in Table 4. Fig. 7 (fold-out) is an example of the 4-week NDVI images for a selected portion for a time series.

Table 4. AVHRR 4-week composite image names, composite start and end date periods and the Hobart internal processing number.

Image Name	Start Date	End Date	Hobart Mosaic #
Jan96	19951230	19960126	129 & 130
Feb96	19960127	19960223	131 & 132
Mar96	19960224	19960322	133 & 134
Apr96	19960323	19960419	135 & 136
May96	19960420	19960517	137 & 138
MJ96	19960518	19960614	139 & 140
June96	19960615	19960712	141 & 142
July96	19960713	19960809	143 & 144
Aug96	19960810	19960906	145 & 146
Sep96	19960907	19961004	147 & 148
Oct96	19961005	19961101	149 & 150
Nov96	19961102	19961129	151 & 152
Dec96	19961130	19961227	153 & 154
Jan97	19961228	19970124	155 & 156
Feb97	19970125	19970221	157 & 158
Mar97	19970222	19970321	159 & 160
Apr97	19970322	19970418	161 & 162
May97	19970419	19970516	163 & 164
MJ97	19970517	19970613	165 & 166
June97	19970614	19970627	167 & 168
July97	19970712	19970808	169 & 170
Aug97	19970809	19970905	171 & 172
Sep97	19970906	19971003	173 & 174
Oct97	19971004	19971031	175 & 176
Nov97	19971101	19971128	177 & 178
Dec97	19971129	19971226	179 & 180
Jan98	19971227	19980123	181 & 182
Feb98	19980124	19980220	183 & 184
Mar98	19980221	19980320	185 & 186
Apr98	19980321	19980417	187 & 188
May98	19980418	19980515	189 & 190
MJ98	19980516	19980612	191 & 192
June98	19980613	19980710	193 & 194
July98	19980711	19980807	195 & 196
Aug98	19980808	19980904	197 & 198
Sep98	19980905	19981002	199 & 200
Oct98	19981003	19981030	201 & 202
Nov98	19981031	19981127	203 & 204
Dec98	19981128	19981225	205 & 206

In Table 4 the composite period is 4 weeks. There are thirteen 4-week periods in a year and only 12 months. To provide meaningful image names we have created a period denoted MJ, which is a period that straddles the end of May and the beginning of June for each year.

Two 4-week composites have been merged based on the maximum NDVI into a 8-week composite, this is listed in Table 5. Fig. 8 (fold-out) is an example of the 4-week NDVI images for a selected portion for a time series.

Table 5. AVHRR 8-week composite image names, composite start and end date periods and the Hobart internal processing number.

Image Name	Start Date	End Date	Hobart Mosaic #
JanFeb96	19951230	19960223	129, 130, 131 & 132
MarApr96	19960224	19960419	133, 134, 135 & 136
MayMJ96	19960420	19960614	137, 138, 139 & 140
JuneJuly96	19960615	19960809	141, 142, 143 & 144
AugSept96	19960810	19961004	145, 146, 147 & 148
OctNov96	19961005	19961129	149, 150, 151 & 152
Dec96Jan97	19961130	19970124	153, 154, 155 & 156
FebMar97	19970125	19970321	157, 158, 159 & 160
AprMay97	19970322	19970516	161, 162, 163 & 164
MJJune97	19970517	19970627	165, 166, 167 & 168
JulyAug97	19970712	19970905	169, 170, 171 & 172
SepOct97	19970906	19971031	173, 174, 175 & 176
NovDec97	19971101	19971226	177, 178, 179 & 180
JanFeb98	19971227	19980220	181, 182, 183 & 184
MarApr98	19980221	19980417	185, 186, 187 & 188
MayMJ98	19980418	19980612	189, 190, 191 & 192
JuneJuly98	19980613	19980807	193, 194, 195 & 196
AugSep98	19980808	19981002	197, 198, 199 & 200
OctNov98	19981003	19981127	201, 202, 203 & 204

Next we describe the format of the AVHRR data. In Section 5 we show how to process the AVHRR data using the teaching manual, specific to ER-Mapper, developed and transferred as part of PNG_DATS.

4.3 Description of the AVHRR Time Series.

This section expands on the notes provided by CSIRO Marine Research when AVHRR composite imagery is purchased from them.

The AVHRR composites are supplied as 11-channel images with 8 bits per pixel, this is referred to as byte data. The data is band interleaved by line or BIL. There is a 512 byte header. Each image for the PNG area contains 11 channels.

The contents of the 11 channels are:
channel 1 bits 7-0 Albedo band 1

channel 2	bits 7-0	Albedo band 2
channel 3	bits 7-0	NDVI
channel 4	bits 7-3	day of the month
channel 4	bits 2-0	cloud indication
channel 5	bits 7-0	satellite direction cosine east
channel 6	bits 7-0	satellite direction cosine north
channel 7	bits 7-0	solar direction cosine north
channel 8	bits 7-0	solar direction cosine Z
channel 9	bits 7-0	Brightness Temp Band 3 - Brightness Temp Band 4
channel 10	bits 7-0	Brightness Temp Band 4
channel 11	bits 7-0	Brightness Temp Band 4 - Brightness Temp Band 5

Channel 1 & Channel 2

These are the albedo for the AVHRR red and NIR channels respectively, see Table 1 for the specific bandwidths, of these AVHRR channels. The interpretation of digital number (DNs) in these channels is listed Appendix 2.

Channel 3

The Normalised Difference Vegetation Index (NDVI), see section 3.1 for a discussion of the form and relationship between NDVI to vegetation parameters, is recovered from channel 3 by using the procedure:

NDVI = (Chn3_DN - 51) / 200.0

The NDVI values can only range between -1.0 and 1.0, due to the form of the equation see section 3.1. However, this data is scaled between -0.25 to 1.0, very little data actually has values between -1 to -0.25.

Channel 4

Contains two parameters in the one channel, these are a cloud mask and the day of the month that contributed the data values for that particular pixel in the composite. These two parameters were placed into one channel to reduce the size of the overall image.

Cloud = modulus (Chn4_DN / 8) the resulting number is between 0 and 7 and is interpreted as

0	clear
1	possibly cloudy
2	(spare)
3-6	cloudy
7	null

Day_of_month = (Chn4_DN / 8) - (modulus [Chn4_DN / 8] /8).

This can be replaced using the Floor arithmetic operator in ER-Mapper, which is given by the following:

Day_of_month = floor(Chn4_DN / 8), this provides the integer part of the number

To fully understand the packing of these two parameters into the one channel lets look at an example, given in Table 6.

Table 6. Example of how to unpack the two parameters stored in Channel 4 and how to interpret each parameter.

Chn_4 DN	Day_of_month When divided by 8	Modulus when divided by 8	Cloud Interpretation
96	12	0	Clear
97	12	1	Possibly Cloud
98	12	2	Spare
99	12	3	Cloudy
100	12	4	Cloudy
101	12	5	Cloudy
102	12	6	Cloudy
103	12	7	Null
104	13	0	Clear
105	13	1	Possibly Cloud

Only pixels which had a cloud flag of 0 (clear) were used in this analysis. Hobart use the cloud flagging algorithm of Saunders and Kriebel (1988), with several minor operational changes (some threshold values are changed and the spatial coherence test is not used; Tildesley *pers. comm*.).

Channel 5,6,7 & 8

Provide direction cosines are recovered from the 8-bit data values by using the procedure: cosine = (ChnX_DN - 128) / 128, where X equals 5,6,7 or 8 depending on the cosine direction which is being calculated.

For either the spacecraft or the sun, the third direction cosine can be calculated from the given two if required. The direction cosines included in the data were selected so as to retain maximum accuracy.

These channels allow the sun-target-sensor geometry to be accurately determined. They have not been used in this project.

Channel 9,10 & 11

Brightness Temperature for Band 4 (in degrees Celsius) is recovered from the 8-bit data value by using the procedure:

Tb4 = Chn10_DN * 0.5 - 63.75

where if the Chn10_DN = 0 then the Tb4 is less than -63.5 (°C), and if Chn10_DN = 255 then this represents a null value. Thus the precision of Tb4 is 0.5 °C for each digital number. The Chn10_DN = 146 converts to Tb4 of 9.25 °C, the actual data range represented by this DN is from 9.25 °C to 9.74 °C. Originally AVHRR data is recorded as 10-bit data (0 to 1023 is the possible range of numbers, this can be represented with no loss of precision by an integer image, 2 bytes per pixel per channel) this allows greater precision than the 8-bit data (0 to 255 is the possible range of numbers, this can be represented by a byte image, one byte per pixel per channel). So while there is a loss of precision in using the byte data the hard disk requirements are halved in comparison to integer data.

5.0 Technical Procedures for Implementing PNG_DATS

5.1 Data Locations

At PNGGS, the **AVHRR** data is in the form of **Ermapper** algorithms, datasets and virtual datasets. The original CSIRO processed **AVHRR** data with **Ermapper** extension files are located on four CD's:

CD #1: 1996 2-week composites
CD #2: 1997 2-week composites
CD #3: 1996 4-week composites
CD #4: 1997 4-week composites, 1998 2-week composites

Functional Ermapper algorithms and virtual datasets are found on PNGGS **PC-Dell** at the file location: **C:\AVHRR** and master copies of these in **C:\AGSO**.

This document is called **manual.doc** located at: **C:\AVHRR\training**

A projection file **lamcon2.txt** is found on **CD #4 F:\text**.

For full functionality of the established AGSO/CSIRO data system, the file **allreal** should be loaded from **CD #3 F:\data**. This file is 239Mb and can be deleted when the system is not in use.

5.2 Receiving NOAA AVHRR data from Tasmania

1. Login to Netscape
2. In the **file** menu select **open location**
3. Type in: 'ftp://ftp.marine.csiro.au'
4. Click on **pub** then **tildesley** then **bierwirth**
5. See Table 4 for desired 4 week data set
6. Click on the desired filename with the right button and select **save link as ..**
7. Choose an appropriate directory and save file

AVHRR data sets are large (22MB) and took more than two hours to receive during testing on the PNGGS system. The 4-week composite naming and start and end dates are listed in Table 4, above.

5.3 Importing into ER-Mapper and using formulas to extract information

The data file imported in section 1 via the internet is the 4 week AVHRR composite product from CSIRO Marine Research. The format is:

Band interleaved by line
Rows = 1170
Columns = 1800
Bands = 11
Datatype = Unsigned 8 bit integer
Header = 512 bytes
Projection = Lambert conformal

1. Use **Windows Explorer** to rename the received file to an appropriate month name, e.g.**apr98**.
2. Load CD # 3
3. Use **Windows Explorer** to copy F:\dat4wk96**jan96.ers** to C:\AVHRR\data and rename to filename.ers, e.g. **apr98.ers**.

All 4 week Ermapper **.ers** files are the same and contain the image and projection information described above.

4.Open a new algorithm window:

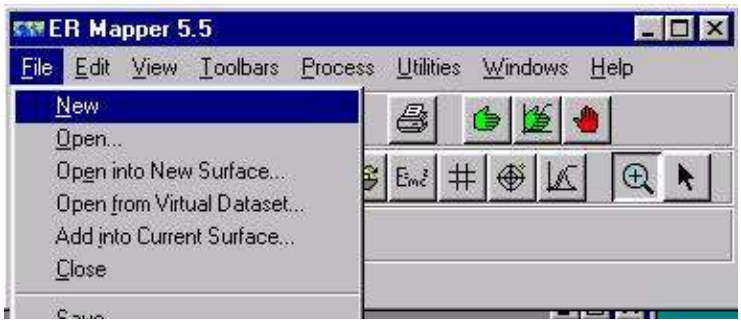

5. From the menu above, select Open
6. From C:\AVHRR\algs, select **layers.alg**
7. From the menu above, select **view** then **algorithm**
8. In algorithm window, **load dataset**:

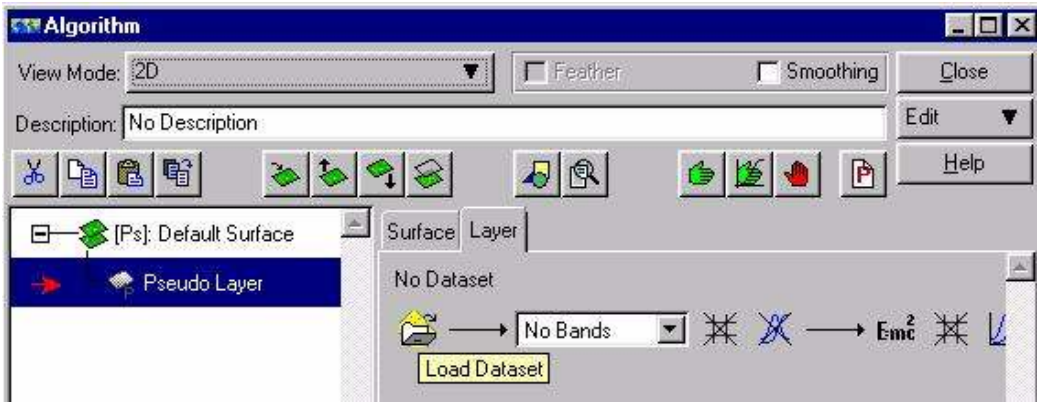

9. Select primary data-set, e.g, **apr98** from C:\AVHRR\data

Various layers are now visible from the AVHRR data:
a) cloud index
b) day of month
c) albedo 1 (derived from AVHRR band 1)
d) albedo 2 (derived from AVHRR band 2)
e) NDVI
f) brightness temperature (AVHRR band 4)

Check the formulas by clicking on formula icon:

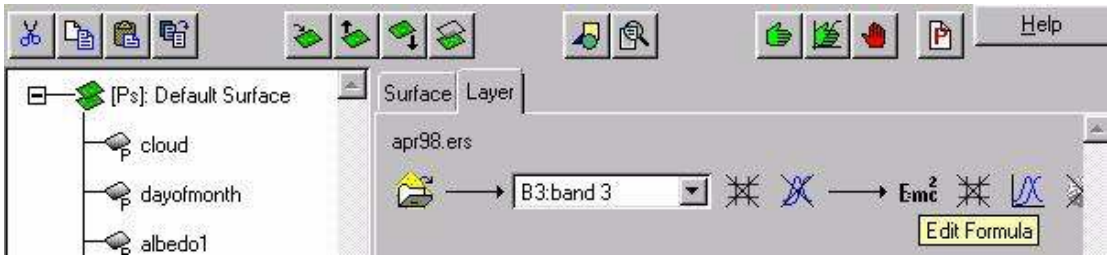

to see how these layers are derived

Information on the primary data layers is contained in Section 4.3. Albedo, NDVI and brightness-temperature are influenced by cloud and the next section deals with masking cloud areas.

5.4 Creating an NDVI algorithm from NOAA/AVHRR 4 week composite images

1. Open a new algorithm window: From the **file** menu, select **New**
2. From the **view** menu select **algorithm**
3. In algorithm window, click on **load dataset icon** (see example above)
4. From C:\AVHRR\data, select **mar98.ers**
5. Click on **Edit Formula** icon:

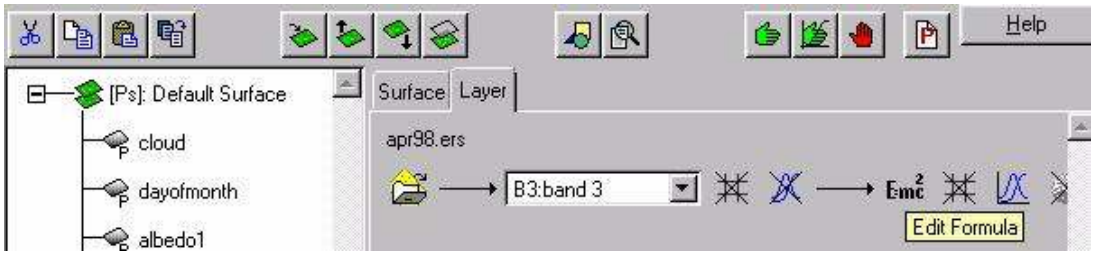

6. Click on **File** and select **Open**:

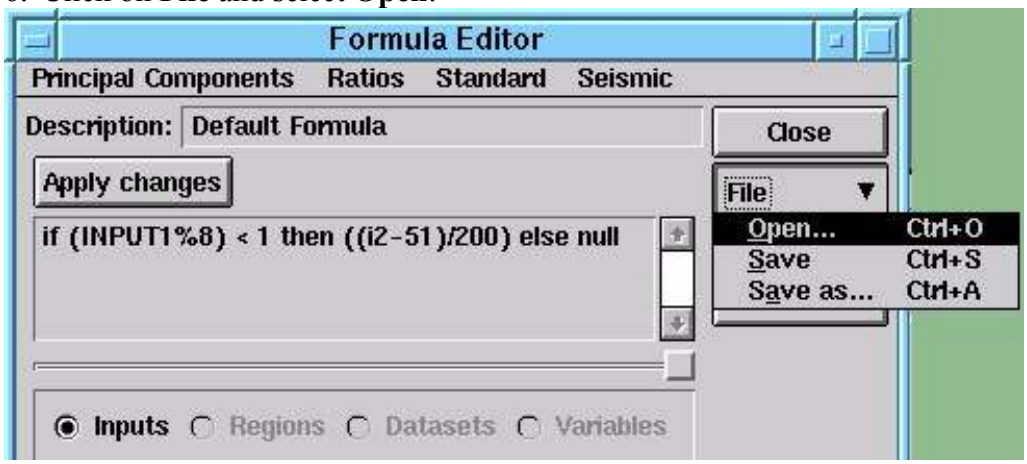

7. Go to **C:\AVHRR\formulas** and select **ndvi.frm** and click **OK**

This formula derives the NDVI vegetation index values from band 3 of the primary dataset for each pixel. It also extracts those pixels determined to be cloudy (see earlier section) and sets them to null which appear black on display.

8. Click on the **Run Algorithm (GO)** icon (green hand)

NDVI values need to be enhanced for display:

9. Click on the **Edit Transform limits** icon:

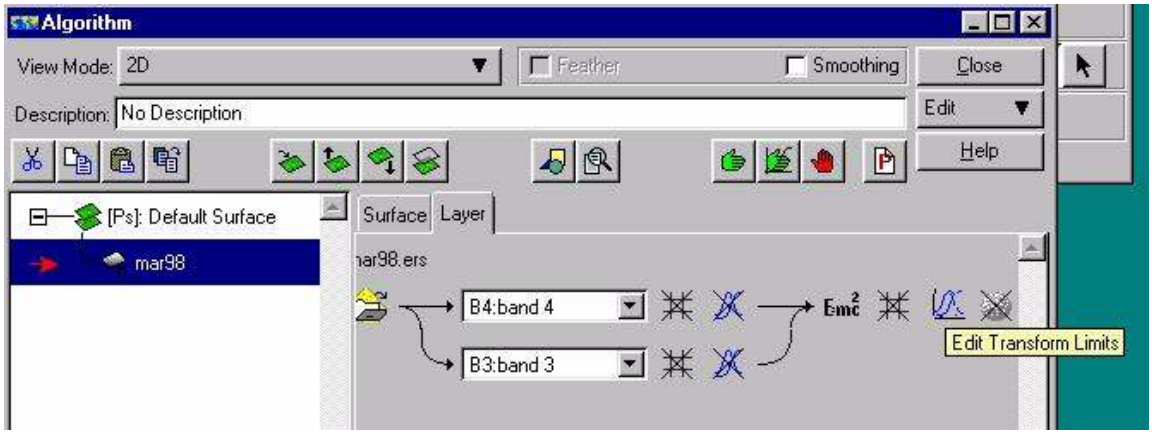

10. Click on **Limits** and select **Limits to Actual**

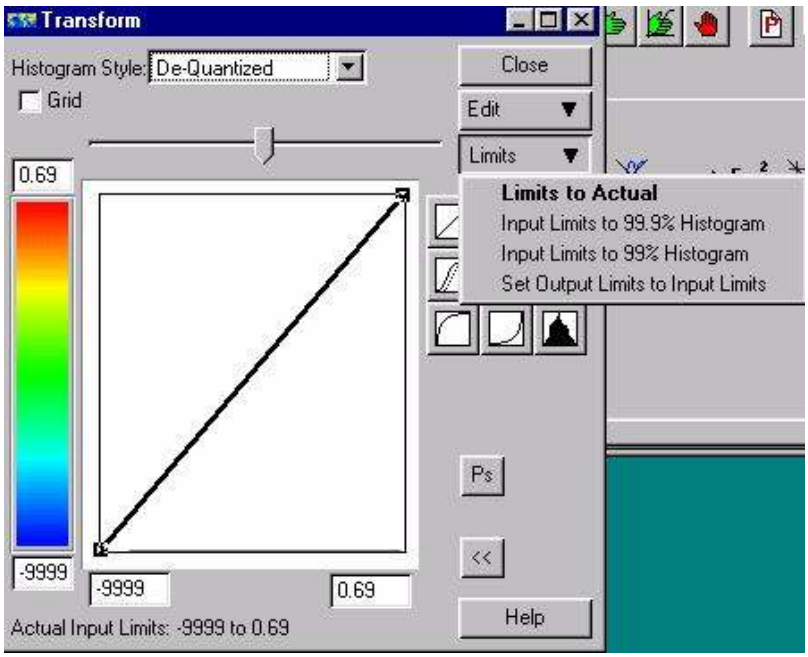

11. Click on the **Run Algorithm (GO)**
12. Manipulate **transform** breakpoints to adjust display colours
13. From the **algorithm window** select **surface** and then **Color Table -** Experiment with look up tables.

5.5 Using the AGSO/CSIRO ER-Mapper algorithm system developed at the PNGGS

Fig. 9 shows how the files are structured to create display and printing algorithms for 4 and 8-week composites and difference images. This is done through a series of Ermapper virtual datasets and algorithms. Formulas for the various steps are embedded in the files.

Because 8-week composite images require a specific data value for cloud areas a new dataset (not virtual) must be created from the primary data sets. To use all the 8-week algorithms and data, the dataset **allreal.ers** and **allreal** must be loaded from **CD # 3**.

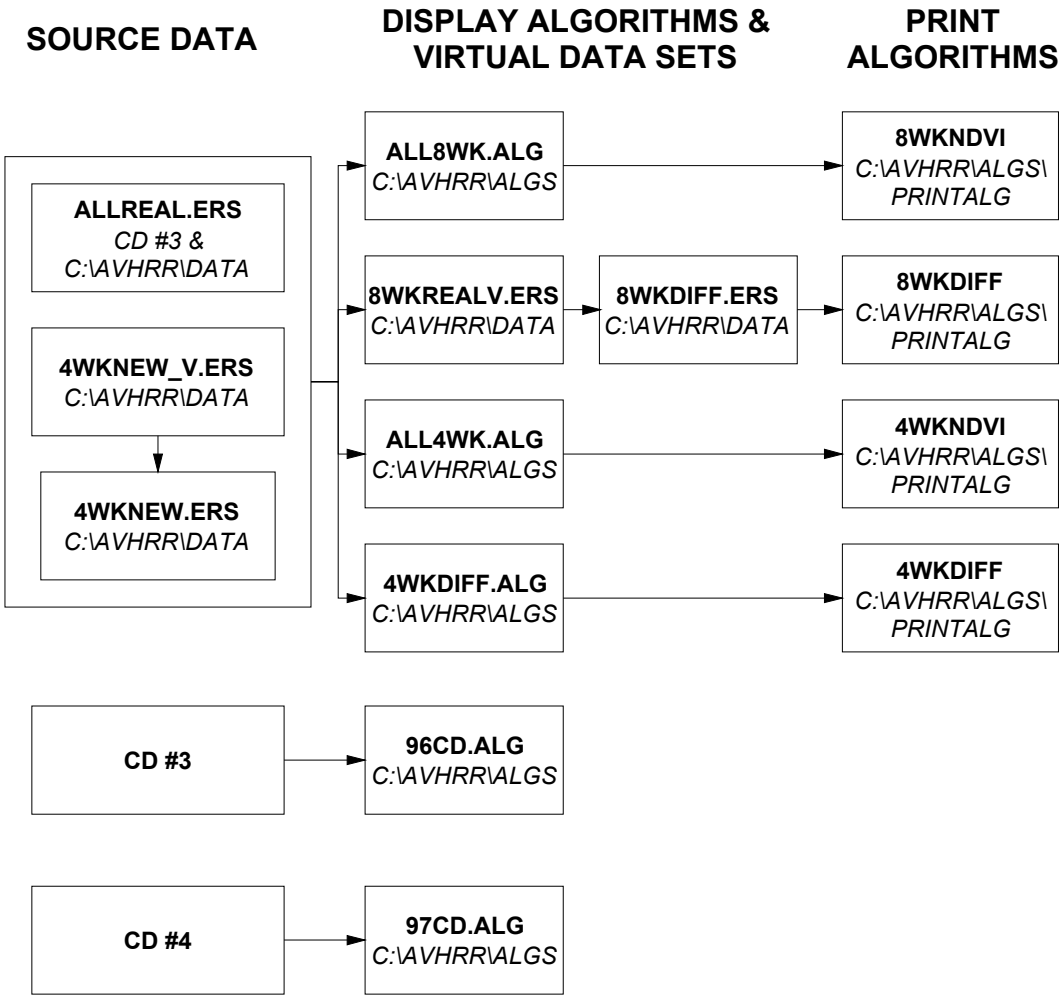

Fig. 9: Flow chart of file structure.

5.5.1 Creating a data-set for new AVHRR data

1. From the **file** menu select **Open from Virtual Dataset**
2. Go to **C:\AVHRR\data** and select **4wknew_v**

This is a virtual dataset to be added to containing the march98 dataset

3. From the **view** menu, select **algorithm**
4. Click on the duplicate icon:

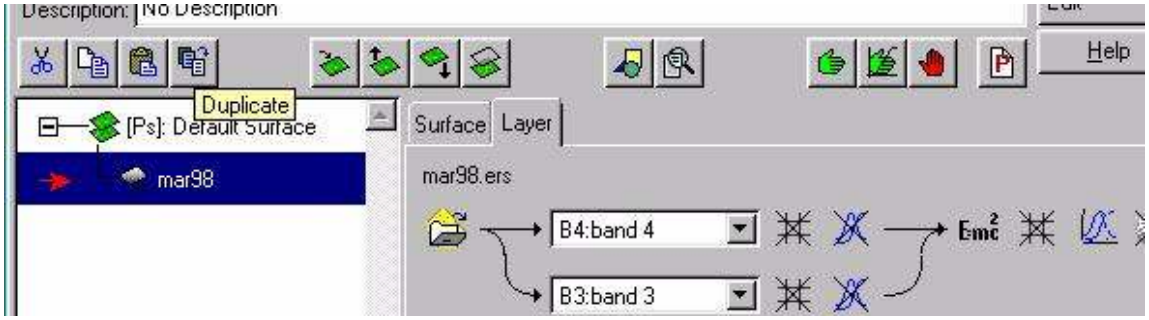

5. Click on **Load Dataset**
6. Select file from **C:\AVHRR\data**, e.g.**apr98.ers** and **OK this layer only**
7. Make sure all layers are turned on and rename the bottom layer on the left-hand side from **mar98** to the new name.
8. Click on the **Run Algorithm (GO)** icon (green hand)
9. Click on the **Edit Transform limits** icon:

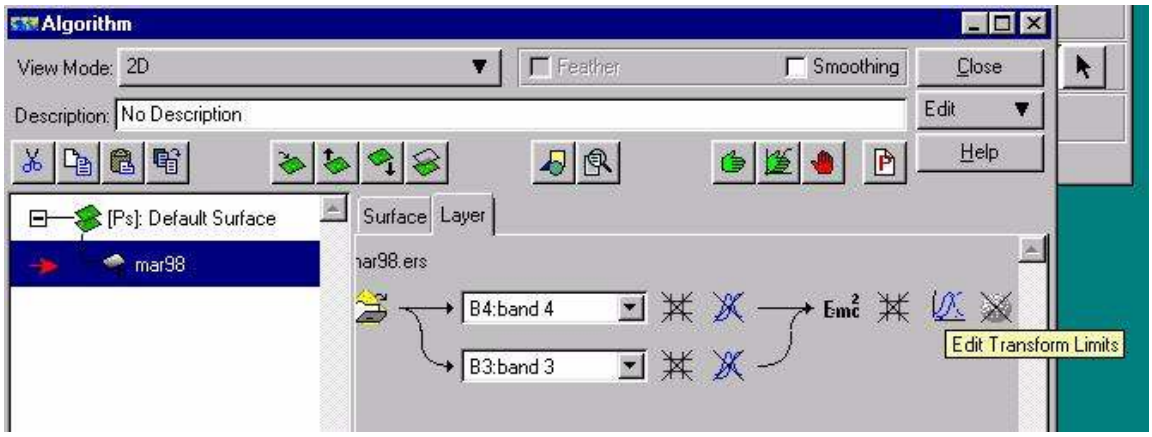

10. Click on the Limits button and then select **Limits to actual**:

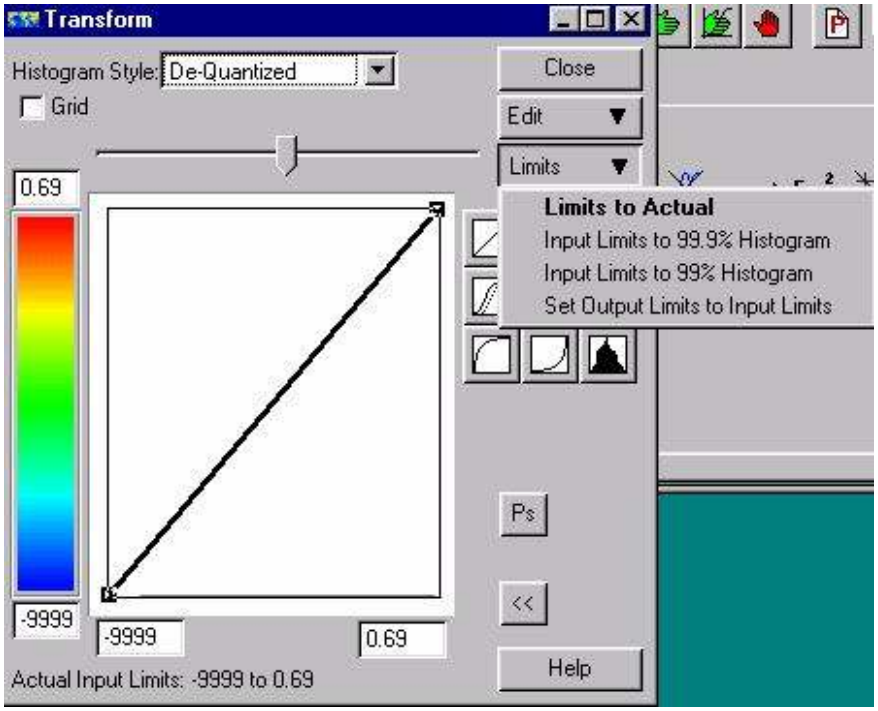

11. Click on the Limits button and then select **Set Output Limits to Input Limits** (this ensures that clouds are saved as a data value of -9999).
12. From the file menu, select **Save as Virtual Dataset**
13. Save as **4wknew_v.ers**
14. From the **file** menu, select **Save as Dataset**
15. In the **Save as Dataset** window choose the following:

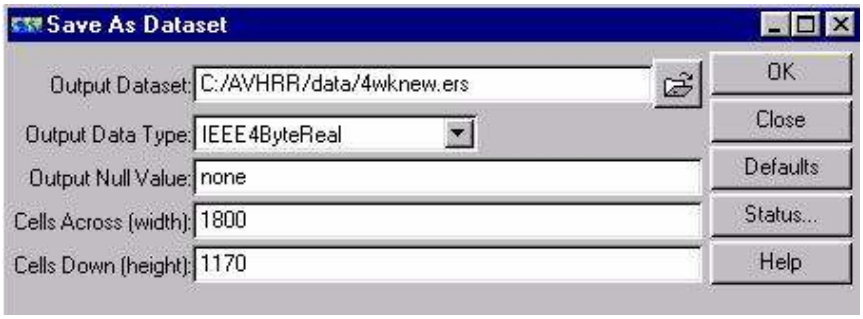

5.5.2 Adding to and creating 4 week composite display and printing algorithms.

1. From the **file** menu select **Open**
5. From C:\AVHRR\algs, select **all4wk.alg**
6. From the menu above, select **view** then **algorithm**
7. Click on the **Duplicate** icon
8. Click on **Load Dataset**
9. Choose **C:\AVHRR\data\4wknew.ers**
10. Load desired monthly NDVI data e.g. **apr98:**

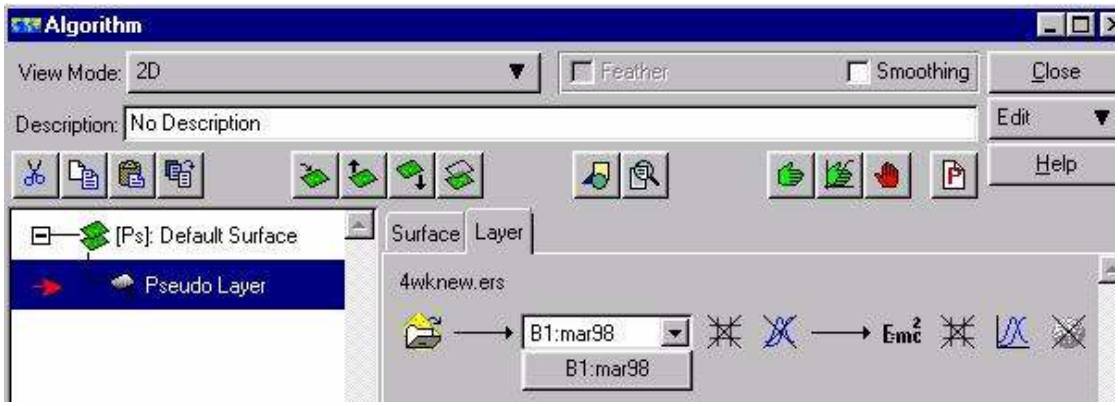

11. Change layer name to new name, eg **apr98**
12. Turn other layers off with the **Turn On/Off** icon

13. From the **file** menu, select **Save as**
14. **C:\AVHRR\algs\all4wk.alg**
15. Click **yes** to overwrite the file (original algorithms can be found in C:\AGSO\algs)
16. From the **file** menu, select **Save as**
17. Go to **C:\AVHRR\algs\printalg\4wkndvi**
18. Save as filename, eg **apr98.alg**

5.5.3 Adding to and creating 4- week difference image display and printing algorithms.

1. From the **file** menu select **Open**
2. From C:\AVHRR\algs, select **4wkdiff.alg**
3. From the menu above, select **view** then **algorithm**
4. Click on the **Duplicate** icon
5. Click on **Load Dataset**
6. Choose **C:\AVHRR\data\4wknew.ers** and **OK this layer only**
7. Load desired monthly NDVI data for differencing e.g. **mar98** and **apr98** to subtract **apr98** from **mar98:**

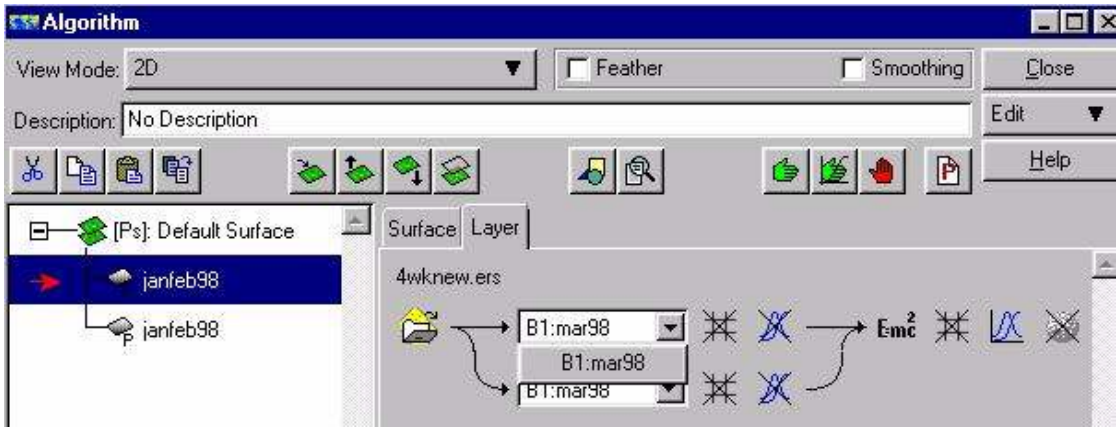

1. Change layer name to new name, eg **marapr98**
2. Turn other layers off with the **Turn On/Off** icon

Note: It is important not to change the transform for one image only as this is used as a standard for image comparisons.

3. From the **file** menu, select **Save as**
4. **C:\AVHRR\algs\4wkdif.alg**
5. Click **yes** to overwrite the file (original algorithms can be found in C:\AGSO\algs)
6. From the **file** menu, select **Save as**
7. Go to **C:\AVHRR\algs\printalg\4wkdiff**
8. Save as filename, eg **marapr98.alg**

5.5.4. Adding to and creating 8-week composite display and printing algorithms.

1. From the **file** menu select **Open**
2. From C:\AVHRR\algs, select **all8wk.alg**
3. From the menu above, select **view** then **algorithm**
4. Turn all layers **off** and go to the bottom 8 week layer, eg **janfeb98**
5. Click on the **Duplicate** icon
6. Click on **Load Dataset**
7. Choose **C:\AVHRR\algs\4wknew.ers**
8. Load desired monthly NDVI data for 2 month composites e.g. **mar98** and **apr98** to composite **apr98** and **mar98.** The formula is set up so that the highest NDVI value is taken so that there is less cloud than in the individual months.
9. Change layer name to new name, eg **marapr98**
10. From the **file** menu, select **Save as**
11. **C:\AVHRR\algs\all8wk.alg**
12. Click **yes** to overwrite the file (original algorithms can be found in C:\AGSO\algs)
13. From the **file** menu, select **Save as**
14. Go to **C:\AVHRR\algs\printalg\8wkndvi**
15. Save as filename, eg **marapr98.alg**

5.5.5 Adding to and creating 8-week difference image display and printing algorithms.

5.5.5.1. Adding to the 8 week composite virtual data-set

1. From the **file** menu select **open from virtual data-set**
2. Go to **C:\AVHRR\data** and select **8wkrealv.ers**
3. From the menu above, select **view** then **algorithm**
4. Go to the bottom 8 week layer, eg **janfeb98**
5. Click on the **Duplicate** icon
6. Click on **Load Dataset**
7. Choose **C:\AVHRR\algs\4wknew.ers**
8. Load desired monthly NDVI data for 2 month composites e.g. **mar98** and **apr98** to composite **apr98** and **mar98.** The formula is set up so that the highest NDVI value is taken so that there is less cloud than in the individual months.
9. Change layer name to new name, eg **marapr98**
10. From the **file** menu, select **Save as Virtual Dataset**
11. **C:\AVHRR\algs\8wkrealv.ers**
12. Click **yes** to overwrite the file (original algorithms can be found in C:\AGSO\algs)

5.5.5.2. Adding to the 8 week difference algorithm

1. From the **file** menu select **Open**
2. From C:\AVHRR\algs, select **8wkdiff.alg**
3. From the menu above, select **view** then **algorithm**
4. Turn all layers **off** and go to the bottom 8 week layer, eg **novdec97-janfeb98**
5. Click on the **Duplicate** icon
6. Load desired monthly NDVI 2 month composites e.g. **janfeb98** and **marapr98** to produce a difference**.** The formula is set up so that **marapr98** will be subtracted from **janfeb98**.
7. Change layer name to new name, eg **janfeb-marapr98**
8. From the **file** menu, select **Save as**
9. **C:\AVHRR\algs\8wkdiff.alg**
10. Click **yes** to overwrite the file (original algorithms can be found in C:\AGSO\algs)
11. From the **file** menu, select **Save as**
12. Go to **C:\AVHRR\algs\printalg\8wkndvi**
13. Save as filename, eg **jf98-ma98.alg**

5.6 Making a poster algorithm

1. Open a new algorithm window: From the **file** menu, select **New**
2. From the **view** menu select **algorithm**
3. In **Algorithm window** click on **Edit** and then **Add Vector Layer,** then **Annotation Map Composition:**

4. Click on **Load Dataset** icon
5. Go to **C:\avhrr\vectors** and select a **.erv** file. Eg. **8wkdiff.erv**
6. Click on **Annotate Vector Layer** icon:

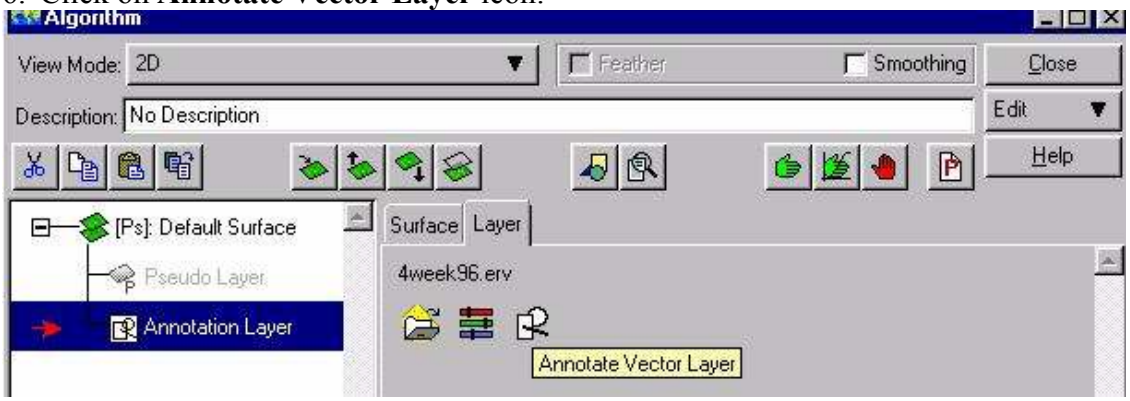

7. Tool icons appear. Click on **Select and Move/Resize Mode**

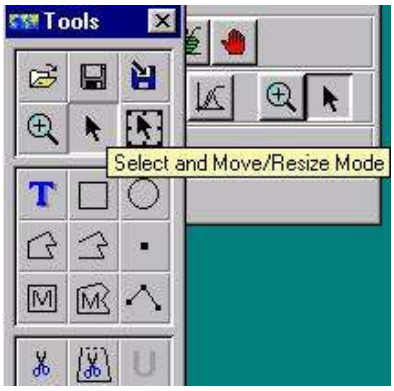

8. Double click on any square in the image

Map Object Attributes and **Map Object Select** boxes appear. Make sure that **Map Object Select Category** equals Algorithm

9. Click on Open Dataset icon next to Algorithm Name:

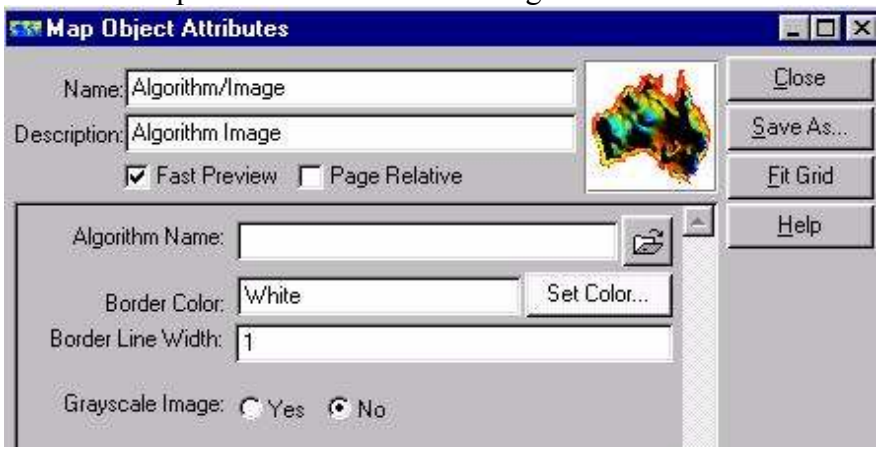

10. Load algorithm to be displayed in selected box. 4 week NDVI data, for example, can be loaded from **C:\AVHRR\algs\printalg\4wkndvi**

11. Select **Close** on **Tools** icon bar
12. Save the vector file
13. Select **Save as** from the **File** menu and save the algorithm.

Image boxes can be resized to fit the image and text can be added in this or another annotation layer. It may be difficult to print a large poster file as large amounts of disk space are required to create a temporary postscript file. One way to get around this is to print to a file:

14. From the **file** menu choose **print**
15. In the **print** window, load the **algorithm** and choose the output name **ER_Mapper.hc**

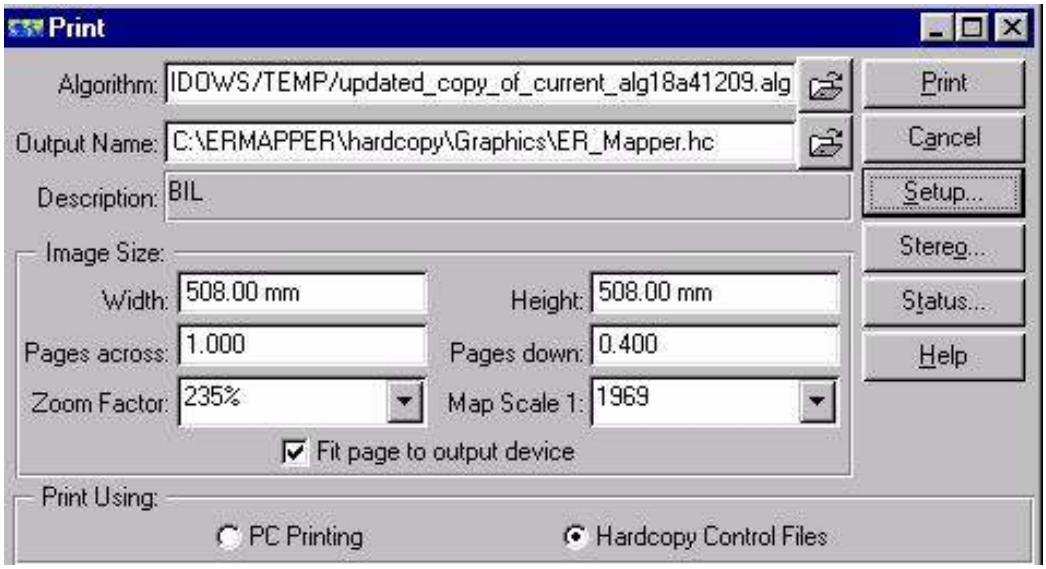

16. Select **hardcopy control Files** and **fit page to output device**
17. Click on **Setup**;

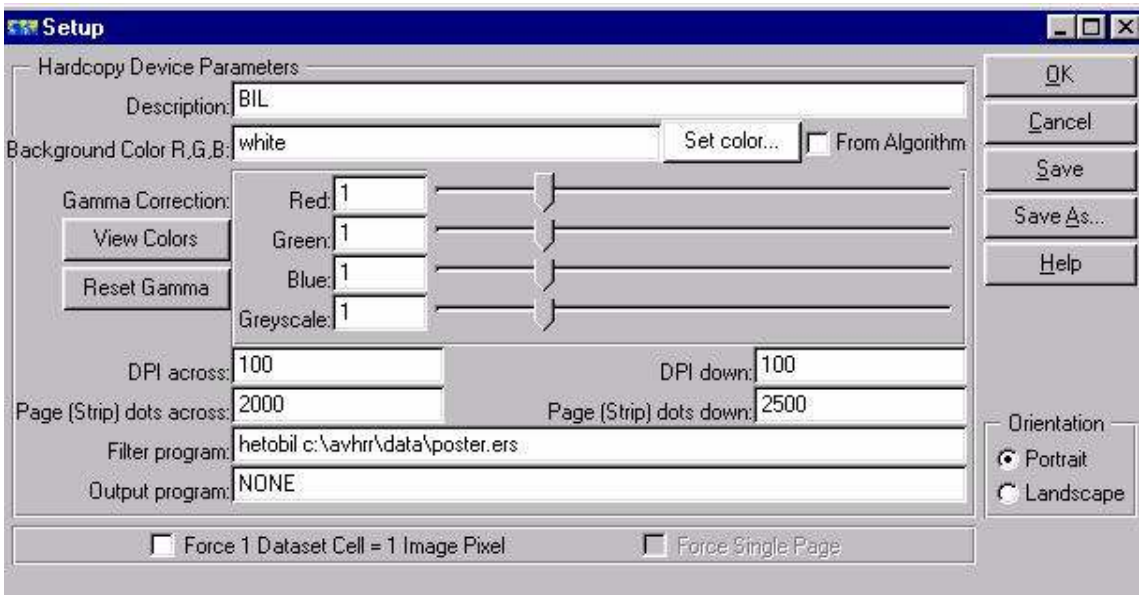

18. Type pathname to dataset in **Filter Program**
19. Insert appropriate image dimensions in **Page dots across** and **down**, e.g, 2000 x 2500.
20. Click **Ok**, then **Print**

The resulting dataset will be 3 band and can be printed when loaded into a standard RGB algorithm

6.0 Analysis of the Remotely Sensed Imagery

6.1 Initial Analysis and Visualization of PNG_DATS

After visually inspecting the different composite images purchased from CSIRO Marine Research Hobart, it was decided that too much cloud was present in the 2-week AVHRR composite for it to be of use in the time series analysis. Consequently, in June 1998 it was recommended to CSIRO Marine Research that 2-week composites for PNG not be produced in the future.

Posters for 4-week data were produced in ER-Mapper, (Fig. 7 and Section 5.6). Visual analysis of the 4-week AVHRR composite data led to a decision to create 8-week composites (Fig. 8 and Section 5.6). These provided promising images.

A difference image is calculated by subtracting the values of one image from another image (Fig. 10 fold out). If there is null data (due to cloud cover) in either image, then this is null in the resulting difference image. Fig. 10a is the 8-week composite data for Sept/Oct period and Fig. 10b is the 8-week composite data for Nov/Dec period. These are the two input images and high NDVI values in both are coloured red and low NDVI values are coloured blue. Fig. 10c is the difference image, red areas indicate a decrease in the NDVI value between the two images and blue areas an increase in the NDVI between the two times. Drought and the associated decrease in vegetation cover is one reason why the NDVI would decrease through time. There are several other factors which causes change in the NDVI signal these include land cover changes and that cloud flagging algorithms may not have sucessfully identified all cloud affected pixels, especially sub-pixel cloud. For example, in Fig. 10c in New Britain some of the small areas where there NDVI values has decreased quickly (the small red areas) may be due to logging operations (McAlpine *pers. comm.*). Field assessments would be needed to confirm this. Also in Fig 10c in Western Province the complex patterns of a high increases and decreases in NDVI are probably due to complex hydrology of that area (Bellamy, 1995).

When dealing with a time series of images it is possible to monitor the trends though time (*e.g.* time1 minus time2; time2 minus time3; time3 minus time4, and so on). To highlight changes in the NDVI signal between consecutive images, difference images were calculated for both the 4-week composite and 8-week composite data (Fig. 11 and 12, respectively both are fold outs). Fig. 12 shows the relative stability of the NDVI signal during 1996 and that there is a large decrease in various locations for different times in the later half of 1997. An increase of the NDVI values, which may be interpreted as a recovery from the drought event is illustrated late in 1997 (Fig. 12). Whether this actually constitutes recovery depends on the definition of drought and may be seen as precurrsive to the subsistence-based agricultural communities having access to normal food supplies. To confirm that food production has returned to normal levels field surveys must be undertaken (Allen and Bourke, 1997, Allen, 1998). Fig. 11 (4-week data) shows a similar trend to Fig. 12 (8-week data). While there is a higher temporal resolution in the 4-week data, there is more cloud present when compared to the 8-week data (Figs 11 and 12).

The mean NDVI and Ts were calculated from the 8-week AVHRR composites for the PNG land area. The mean Ts increases slightly earlier than the mean NDVI decreases at the height of the 1997 drought event; which occurred in the later half of 1997 (Fig. 13.1). In the early part of 1997 the mean NDVI actually increases. During 1996, a year which received average rainfall, the NDVI also increased slightly early in the year. However, these perturbations are minor compared to the large increase in Ts and decrease in NDVI associated with the 1997 drought event (Fig. 13.1). The date for each composite image plotted on the x-axis of the time series plot is the central date of the composite period.

To provide a finer time step when focusing on drought onset and recovery we explored the use of the 4-week composite data from 1997. Using a longer composite period causes the amplitude in the signal of NDVI and Ts to be dampened (compare Figs 13.1 and 13.2). Based on these results we decided to use the 8-week AVHRR data for 1996 and the 4-week data for 1997 and 1998. This pragmatic approach uses AVHRR data with a shorter composite period, when low amounts of cloud cover existed due to drought. An analysis over a longer time period of the drought recovery phase may require using 8-week composite data during 1998. During Jan97 and Feb97 AVHRR data collected had high amounts of cloud contaminated pixels. The percentage of valid data for the 4-week composites during the rest of 1997 is similar to that for the 8-week composite data (Fig. 14.1 and 14.2).

Fig. 13.1 shows that local maxima of Ts coincide with the equinox (March and September) for both 1996 and 1997. This is due to increased solar loading at these times in equatorial countries, like PNG. The Normalised Difference Temperature Index (NDTI), jointly developed by McVicar *et al*. (1992) and Jupp *et al.* (1998), provides a means to normalise for both daily (changes in atmospheric transmittance) and seasonal (earth-sun distances) influences of net radiation. The NDTI requires daily rainfall and extremes of air temperature; this daily meteorological data was not available for this study. During 1997 both Figs 13.1 and 13.2 show a lag between the time of maximum Ts and the time of minimum NDVI. This pattern is due to Ts being influenced by both net radiation and available soil moisture and the NDVI reflecting a lag between vegetation response of conditions (Goetz, 1997). The NDTI provides a method for separating the influence of net radiation and moisture availability in Ts. McVicar and Jupp (1998) suggest that using the resource availability and resource utilisation can be mapped using the NDTI and NDVI, respectively.

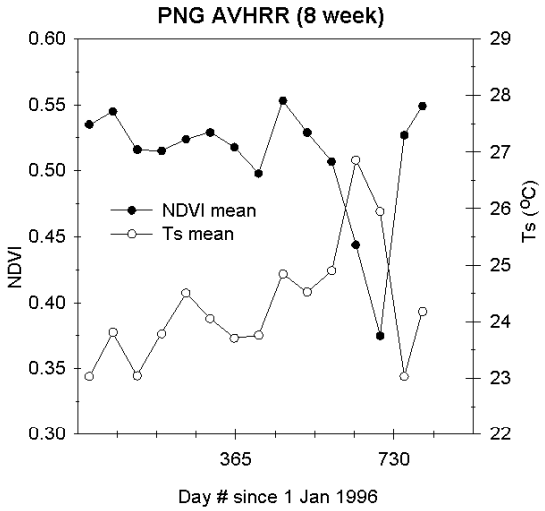

Fig. 13.1: Plot of day since 1 Jan 1996 and NDVI mean and Ts mean for 8-week AVHRR composites.

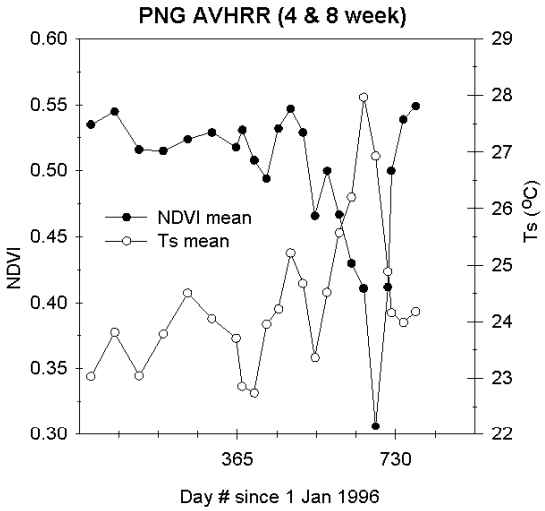

Fig. 13.2: Plot of day since 1 Jan 1996 and NDVI mean and Ts mean for 4-week and 8-week AVHRR composites.

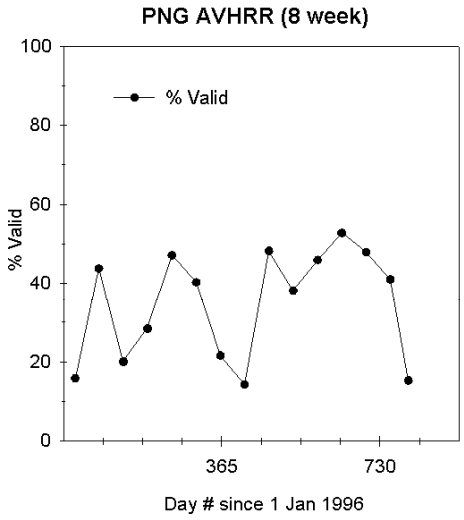

Fig. 14.1: Plot of day since 1 Jan 1996 and % Valid Data for 8-week AVHRR composites.

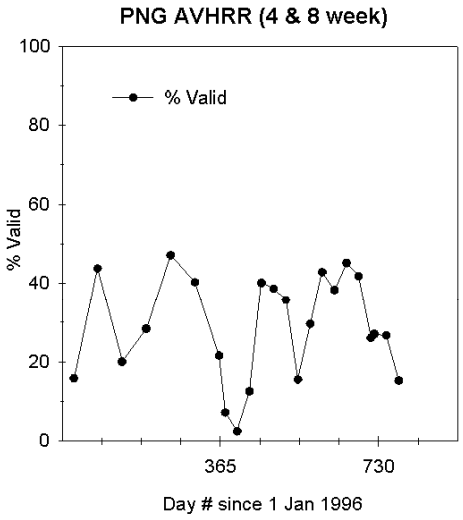

Fig. 14.2: Plot of day since 1 Jan 1996 and % Valid Data for 4-week and 8-week AVHRR composites.

Fig. 13.1 and 13.2 show that Ts and NDVI are negatively correlated. Many previous researchers have related this to estimating ET, partitioning of energy balance components, estimation of surface moisture status and land cover classification. General applications of the combined use of Ts and NDVI are referred to by Goetz (1997); and for discussion of the combined use of Ts and NDVI relevant to drought refer to McVicar and Jupp (1998). Goetz

(1997) reported that the negative correlation between Ts and NDVI, observed at several remotely sensed scales (25 m^2 to 1.2 km^2), was largely due to changes in vegetation cover and soil moisture. Held *et al*. (1995) used a ratio of Ts/NDVI as the spatial backbone to extrapolate a single ground based measurement of ET to a LANDSAT TM quarter scene (90 km^2). For complete canopies, the slope of the T_s/NDVI relationship has been related to canopy resistance (Nemani and Running, 1989, Sellers, 1987, Hope, 1988). Nemani *et al*. (1993) found the slope of T_s/NDVI to be negatively correlated to crop-moisture index. Currently, advances are being made that use the T_s/NDVI plot, combined with meteorological data and process based models to provide a more mechanistic interpretation of the remotely sensed data. There are two methods currently being put forward. The first, is a progression from the slope of T_s/NDVI approach, which describes the data as falling into a triangle (Gillies and Carlson, 1995, Gillies *et al.*, 1997, Carlson *et al.*, 1990, Carlson *et al.*, 1994, Price, 1990). The second, the Vegetation Index / Temperature Trapezoid (VITT) (Moran *et al.*, 1994, Moran *et al.*, 1996, Yang *et al.*, 1997), is an evolution of the Crop Water Stress Index (CWSI), which promotes the idea of data falling into a trapezoid. Both of these techniques require ancillary meteorological data to spatially distribute inferences about the surface energy balance fluxes, or moisture availability. Full descriptions of each of these approaches, and their advantages and disadvantages for operational drought assessment are given in a review by McVicar and Jupp (1998).

For this study in PNG, which was aimed at providing a rapid assessment of the 1997 drought conditions, daily meteorological data was not available. Consequently we had to develop a system which could be based primarily on remotely sensed data. To perform this, and to utlise the negative correlation between Ts and NDVI data, we divided Ts by NDVI. This ratio (Ts/NDVI) becomes higher during times of stress, due to the decrease in NDVI associated with lower plant cover, and the increase in Ts associated with more of the ground surface available energy being partitioned into the sensible heat flux (Fig. 15.1 and 15.2). The time series of Ts/NDVI is an indicator of environmental stress, associated with the 1997 drought conditions in PNG. It does not attempt to provide estimates of the Bowen ratio (the ratio of the sensible heat flux divided by the latent energy heat flux) or provide an input parameter to regional ET modelling.

Longer composite periods dampens the signal of the Ts/NDVI ratio. To observe this dampening effect, compare 1997 in Fig. 15.1 (8-week composites) with 1997 in Fig. 15.2 (4-week composites). In both Fig. 15.1 and 15.2 there is an increase in Ts/NDVI associated with the 1997 drought event. However, in Fig. 15.2 the increase of Ts/NDVI is larger. This increase results because composites are formed based on the maximum NDVI during the period (Section 4.1). Consequently a shorter composite period (in which a lower NDVI data that is cloud free is acquired) means that higher Ts/NDVI values associated with the 1997 drought in PNG will be observed.

During the height of the drought an individual cloud free image may have been acquired which had lower NDVI value than the image used in the composite. However, due to compositing based on the maximum NDVI, this hypothetical image would not be used in the composite. This means that there may be an individual image with a higher Ts/NDVI ratio than is presented here using the composite data.

The next task was to asses differences in the intensity and timing of the 1997 drought event, as monitored by the Ts/NDVI ratio, for different regions within PNG. The regions selected

were provinces, as other ancillary GIS data for the stratification of PNG was not available in a suitable format during the time of this project.

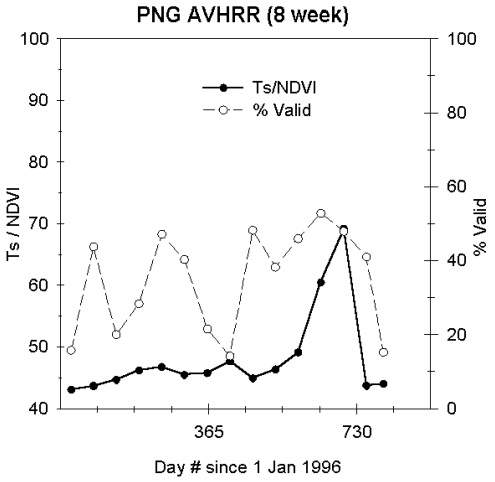

Fig. 15.1: Plot of day since 1 Jan 1996 and mean value of Ts/NDVI for 8-week AVHRR composites.

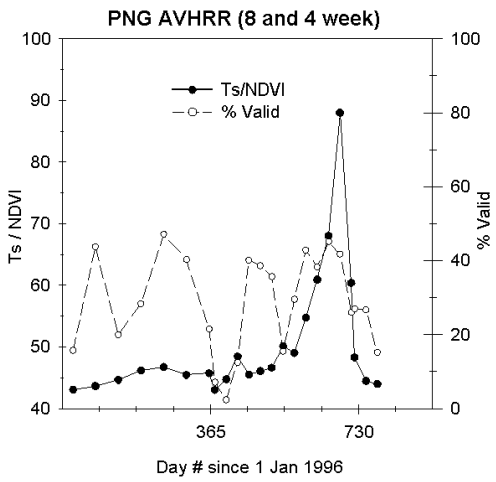

Fig. 15.2: Plot of day since 1 Jan 1996 and mean value of Ts/NDVI for 4-week and 8-week AVHRR composites.

Fig. 14.1, 14.2, 15.1 and 15.2 show the mean response for all data for PNG. Some areas, mainly the highlands, were always cloudy (Fig. 11 and 12). When focusing on these areas it appears to be necessary to use LANDSAT TM or RADAR images. LANDSAT TM has an overpass time of 9:30 am which may be acquired prior to afternoon cloud building up, and after morning fog in the valleys has 'burnt-off'. The repeat cycle of LANDSAT TM is every 16 days, which means that cloud free data may be acquired less frequently than the afternoon AVHRR data presented here. This depends on whether clouds build-up during the day are always present. McAlpine *et al*. (1983) presented data for cloudiness per fortnight. This shows that there is less cloud during May to August (the 'south-east' season). Differences in cloud cover recorded at 0900 and 1500 for the 6 stations reveals complex relationships between daily cycle of local effects and regional scale seasonaility (McAlpine *et al.*, 1983). No generic rules for all of PNG can be provided for morning and afternoon cloudiness patterns. For small areas of the PNG Highlands, it would be best to assess the cloudiness from quick-looks of LANDSAT TM imagery. Cloudiness is important for remotely sensed scene selection (Currey *et al.*, 1987, McGwire, 1998). Airborne RADAR imagery has the capacity to map soil moisture for small area catchments. However, current RADAR data available from satellite sources appear to be hampered by a lack of polarization and wavelengths to reliably determine soil moisture (McVicar and Jupp, 1998).

6.2 Exploring the data at the Province Level

To assess and monitor regional variations in the onset, recovery and severity of the 1997 drought event, we generated time series statistics of Ts/NDVI for each of the 14 mainland provinces.

6.2.1 Southern Region

There are five provinces which comprise the Southern Region. These are Western, Gulf, Central, Milne Bay and Northern (Fig. 1). Western Province (Fig. 16.1) was the worst affected province, as measured by the Ts/NDVI ratio. Central Province (Fig. 16.3) was also badly affected by the 1997 drought event. During 1997 it appears that Milne Bay (Fig. 16.4) may have suffered a longer period of dry conditions compared with the response recorded for Gulf Province (Fig. 16.2). This agrees with the finding of of ground based drought assessment (Allen *et al.*, 1997).

Milne Bay Province (Fig. 16.4) also experienced a slight increase in stress in the middle of 1996, a year during which most of PNG received average rainfall. The increase in Ts/NDVI for Milne Bay Province for 1996 may be associated with marked rainfall seasonality. Frequently small perturbations of Ts/NDVI occur when the proportion of valid data for the province decreases below 10%. This can especially be seen in the plot for Northern Province (16.5). For the first year of data, the ratio is fairly stable (indicating that drought conditions were not experienced during that year as average rainfall was received in 1996) and the proportion of valid data is generally larger than 30%. However, early in the second year of analysis, a small decrease can be seen associated with a very low proportion of valid data for that province. When the proportion of valid data is low for other Southern Provinces small perturbations can also be seen.

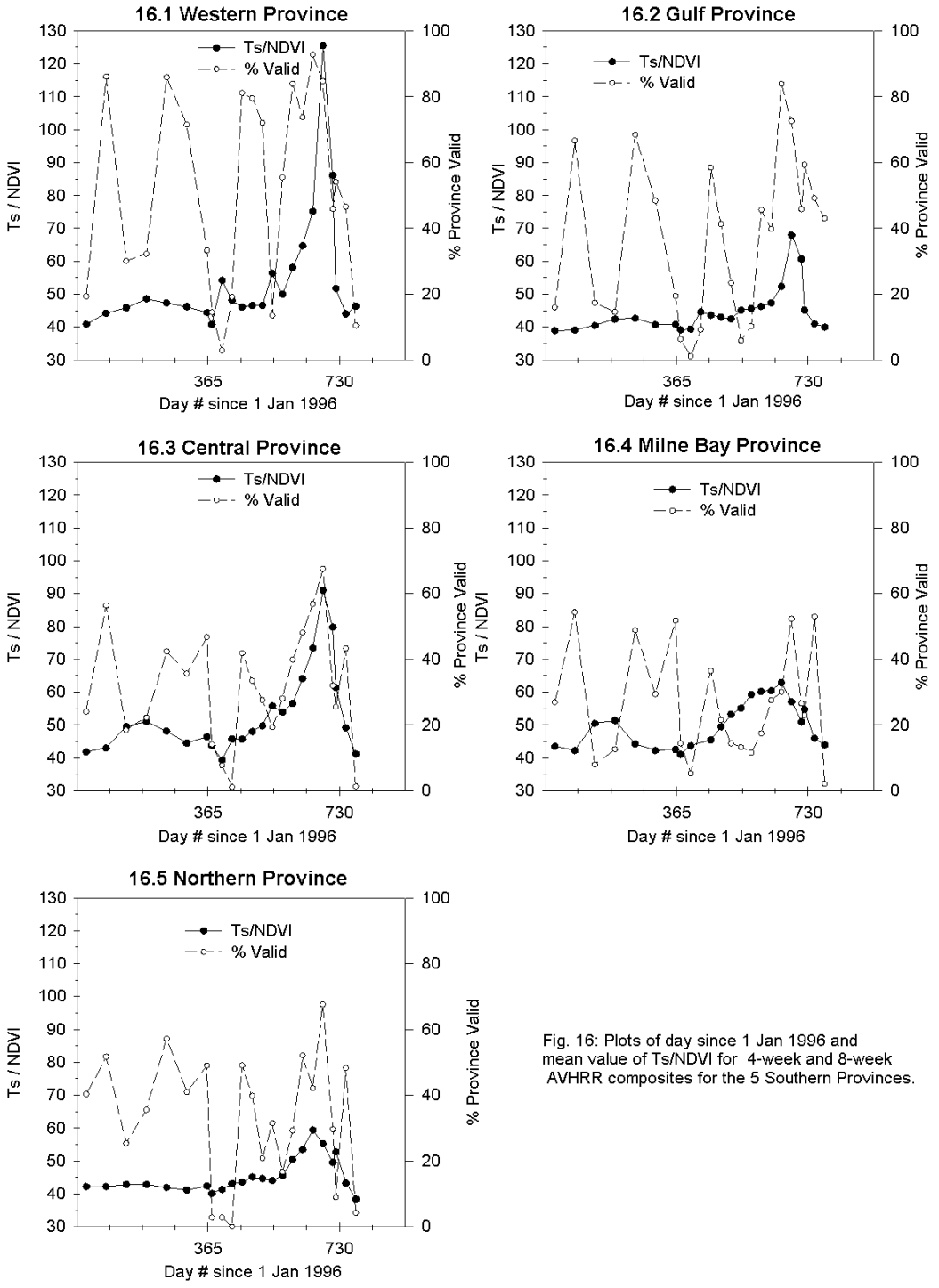

Fig. 16: Plots of day since 1 Jan 1996 and mean value of Ts/NDVI for 4-week and 8-week AVHRR composites for the 5 Southern Provinces.

6.2.2 Highland Region

There are five provinces which comprise the Highland Region. These are Southern Highlands, Enga, Western Highlands, Chimbu and Eastern Highlands (Fig. 1). From Fig. 17 it can be seen that both Chimbu Province and Eastern Highlands Province were the worst affected, as measured by the Ts/NDVI value. The other 3 provinces all show response in the

Ts/NDVI ratio during the 1997 drought event. For all of the Provinces there is a slight increase in the Ts/NDVI ratio during August - November 1996. Rainfall seasonality experienced in the provinces is primarily a Jan-Apr maxima (McAlpine, 1995), which agrees with the trends shown in Fig. 17. It is also interesting to note that for Eastern Highlands Province the base value of Ts/NDVI is higher when compared to the other 4 Highland Provinces. This indicates that this province generally receive less rainfall than the other Highland Provinces (Bourke, 1988). The increase is stress, revealed by the baseline during 1996 of Ts/NDVI and by the magnitude of the ratio during 1997 for both Eastern Highlands Province and Chimbu Province is confirmed by the rainfall being lower in the eastern Highlands and tending to increase in a westerly direction (Bourke, 1988, p.10). The main other environmental factors which could control this response soils (mainly ash) and topography (ranging from flat valley to very steep slopes) are generally the same over the entire highland region (Bourke *pers. comm*.).

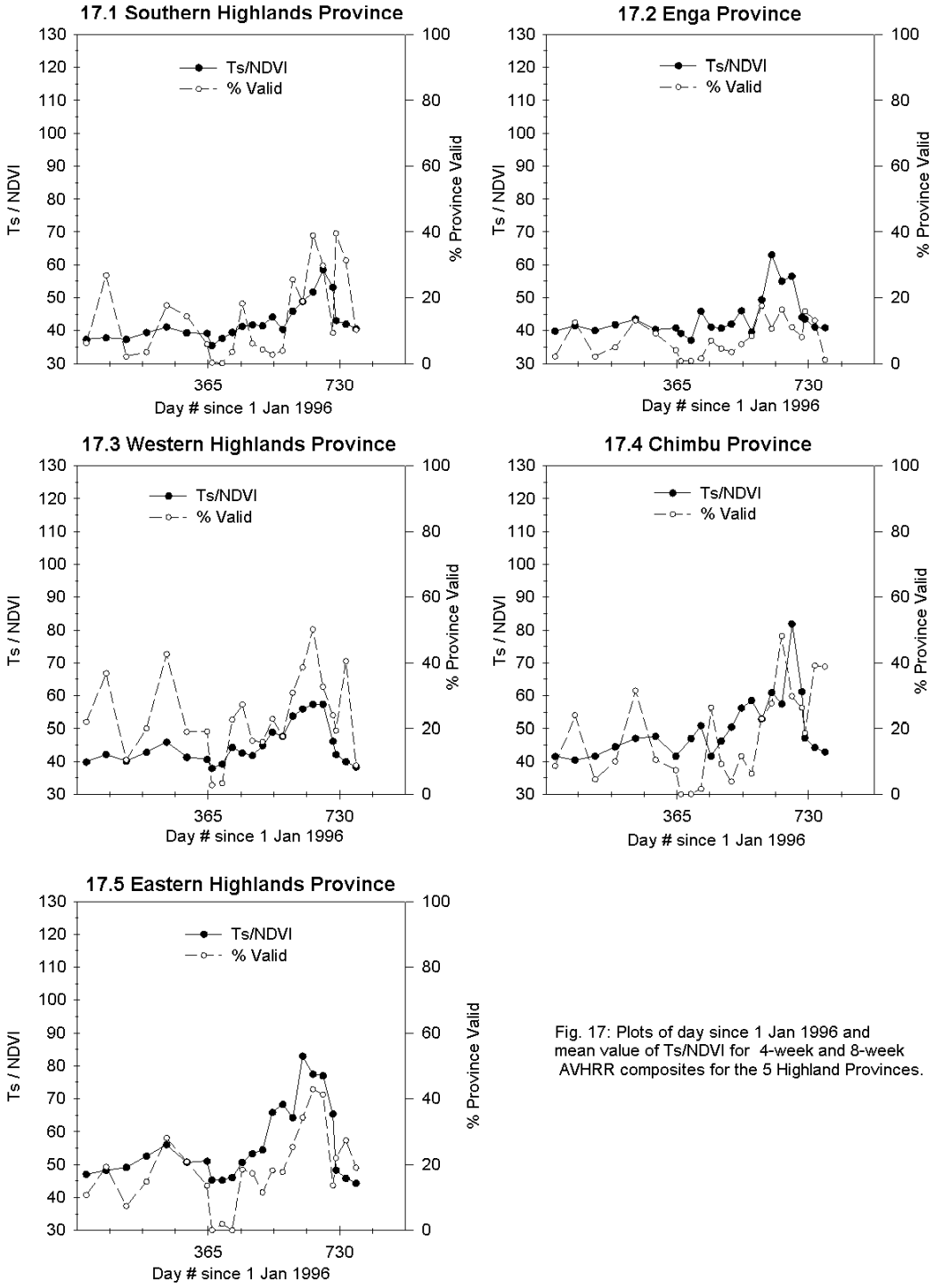

Fig. 17: Plots of day since 1 Jan 1996 and mean value of Ts/NDVI for 4-week and 8-week AVHRR composites for the 5 Highland Provinces.

6.2.3 Mamose Region

There are four provinces which comprise the Mamose Region. These are Morobe, Madang, East Sepik and West Sepik (Fig. 1). Morobe Province (Fig. 18.1) suffered a more intense (the Ts/NDVI value was higher) and longer (the Ts/NDVI value is higher than 50 for a longer

period) drought in 1997 than the other provinces in this region. Madang (Fig. 18.2) experienced stress, due to the 1997 drought, as indicated by the Ts/NDVI value increasing sharply in the later half of 1997. East Sepik Province (Fig. 18.3) was moderately affected, and West Sepik Province (Fig. 18.4) only slightly influenced, by the 1997 drought, as measured by the Ts/NDVI ratio. This agrees with the finding of of ground based drought assessment (Allen *et al.*, 1997).

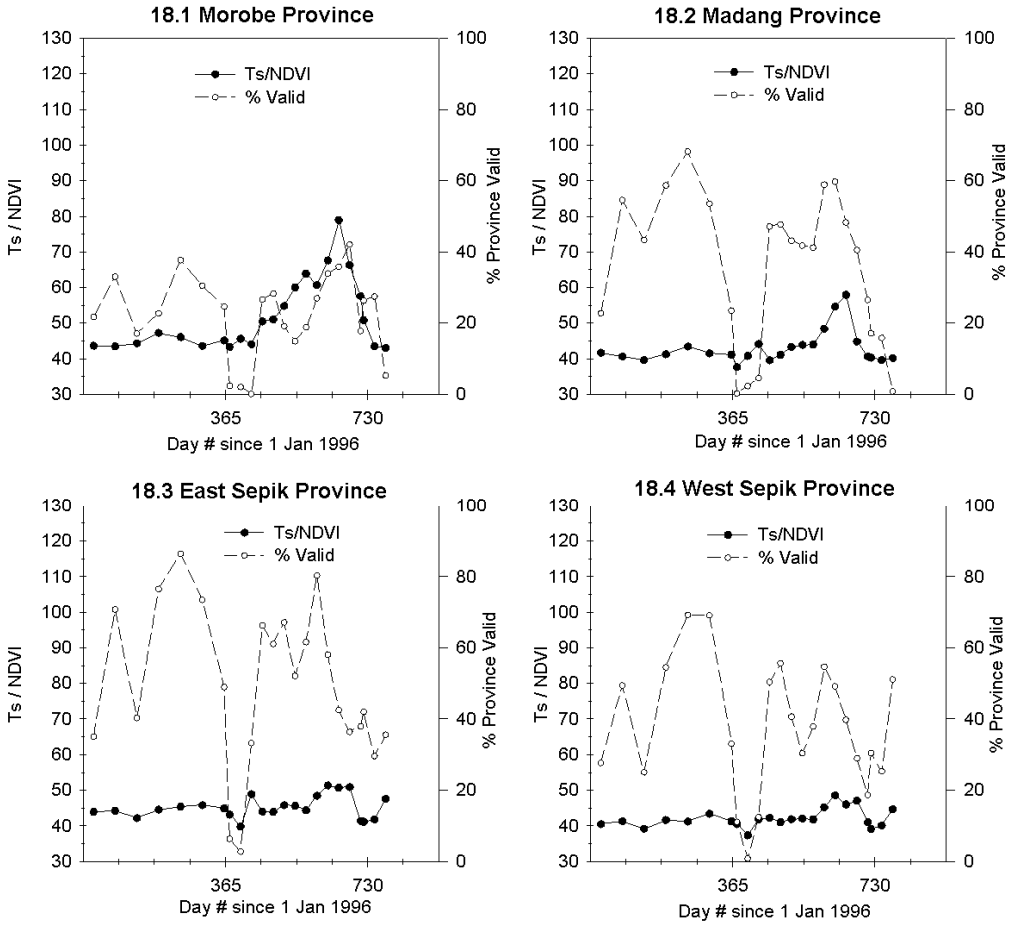

Fig. 18: Plots of day since 1 Jan 1996 and mean value of Ts/NDVI for 4-week and 8-week AVHRR composites for the 5 Mamose Provinces.

6.2.4 Provinces of Interest

The vast differences in the response of Ts/NDVI for 4 provinces of interest is shown in Fig. 19. From this plot it can be seen that Western Province experienced the most intense drought during 1997 (Fig. 19.1). Milne Bay Province (Fig. 19.2) suffered a prolonged period in 1997 where dry conditions occurred. However, Milne Bay Province also seemed to have experienced a dry period in 1996, which may have been associated with rains occurring late in the May-August rainfall maxima (McAlpine, 1995). East Highlands Province (Fig. 19.3) experienced drought in 1997 as indicated by the long period when the Ts/NDVI signal is

high. West Sepik Province (Fig. 19.4) did not experience severe drought conditions in 1997, demonstrated by the low values of the Ts/NDVI signal.

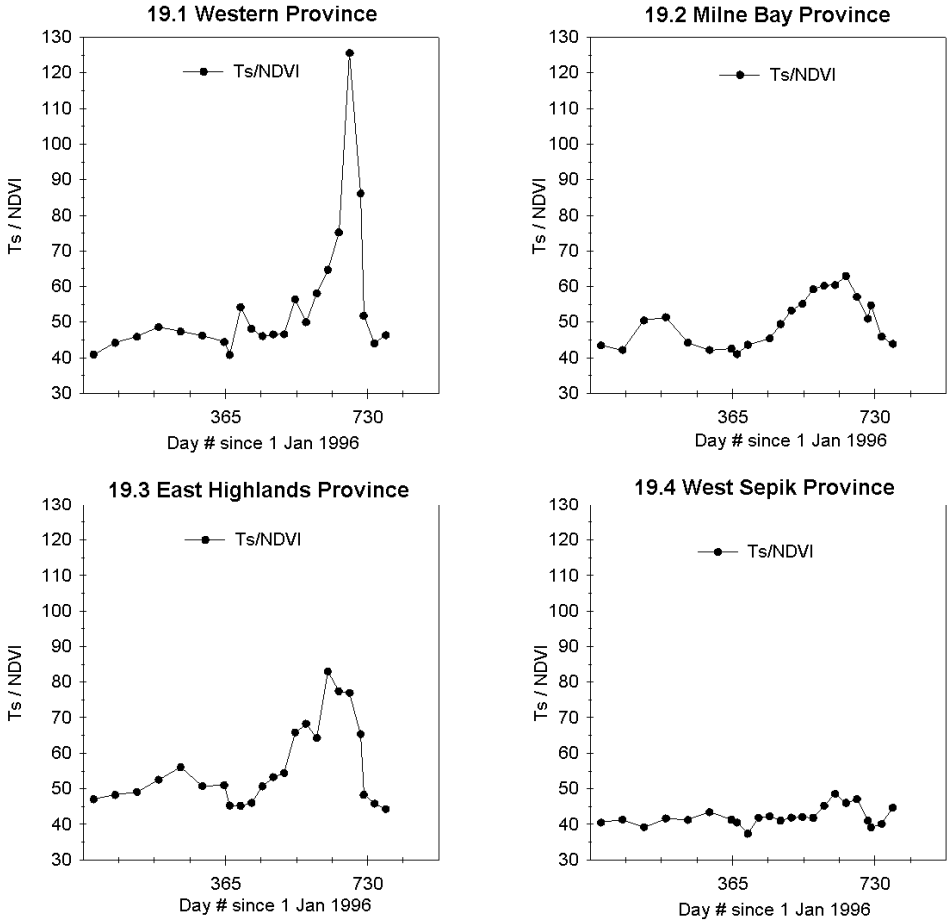

Fig. 19: Plots of day since 1 Jan 1996 and mean value of Ts/NDVI for 4-week and 8-week AVHRR composites for selected Provinces.

6.3 Combining the data with meteorological data sets

Monthly rainfall recorded at the meteorological stations shown in Fig. 1 was available from Jan 1997 until April 1998. However, during this period not all stations had complete monthly rainfall records. Several of the stations that experienced severe drought conditions, not providing data (Miaha *pers. comm*). This provides strong support for field visits and the use of remotely sensed data to assess the drought conditions. At the meteorological stations we were able to extract the Ts/NDVI values for an area 99 by 99 pixels, with the station being centrally in this area.

Fig. 20.1, 21.1 and 22.1 are plots of Ts/NDVI (left hand Y-axis) for the area surrounding the station and monthly rainfall (right hand Y-axis) against time for Kiunga, Wewak and Nadzab, respectively. The plots show that Kiunga received more rainfall than Wewak and Nadzab during 1997. The integral under the plot of Ts/NDVI is a reciprocal of this. Figs 20.2, 21.2

and 22.2 are plots of Ts/NDVI (left hand Y-axis) for the area surrounding the station and percent monthly average rainfall (right hand Y-axis) against time. These plots do not show the same strong relationship as the monthly rainfall plots.

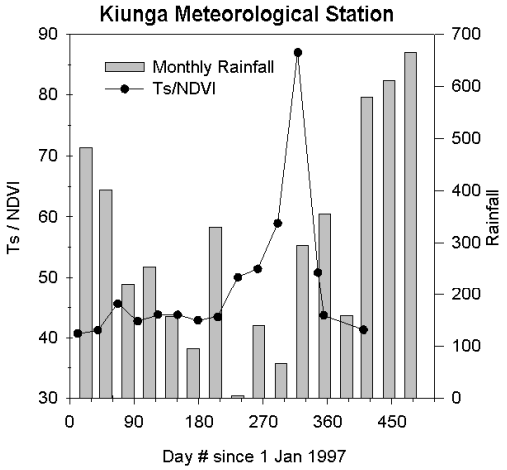

Fig. 20.1: Mean Ts/NDVI for the Kiunga region, derived from 4-week AVHRR composites, and monthly rainfall measured at Kiunga since 1 Jan 1997.

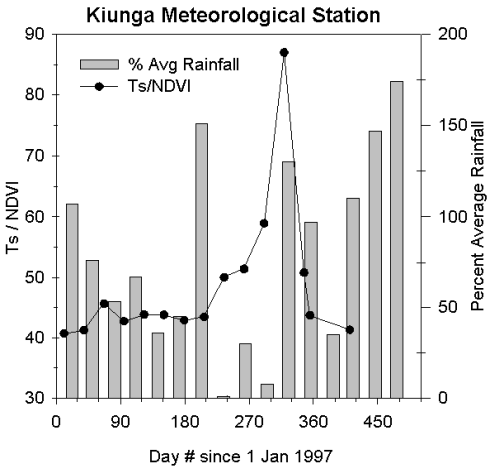

Fig. 20.2: Mean Ts/NDVI for the Kiunga region, derived from 4-week AVHRR composites, and percent average monthly rainfall for Kiunga since 1 Jan 1997.

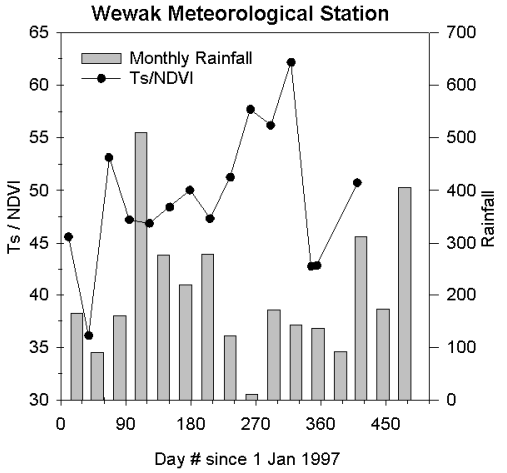

Fig. 21.1: Mean Ts/NDVI for the Wewak region, derived from 4-week AVHRR composites, and monthly rainfall measured at Wewak since 1 Jan 1997.

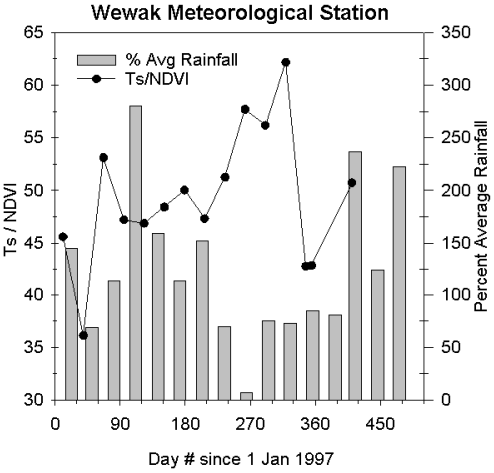

Fig. 21.2: Mean Ts/NDVI for the Wewak region, derived from 4-week AVHRR composites, and percent average monthly rainfall for Wewak since 1 Jan 1997.

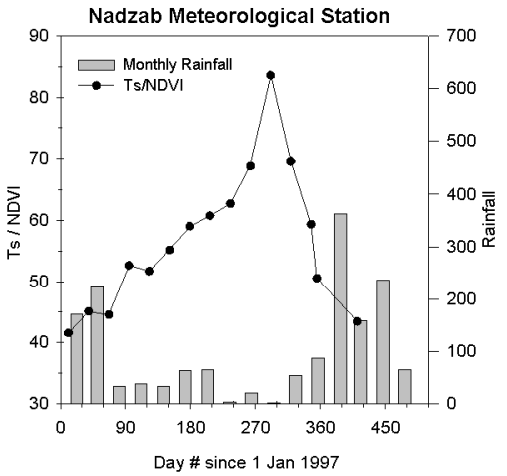

Fig. 22.1: Mean Ts/NDVI for the Nadzab region, derived from 4-week AVHRR composites, and monthly rainfall measured at Nadzab since 1 Jan 1997.

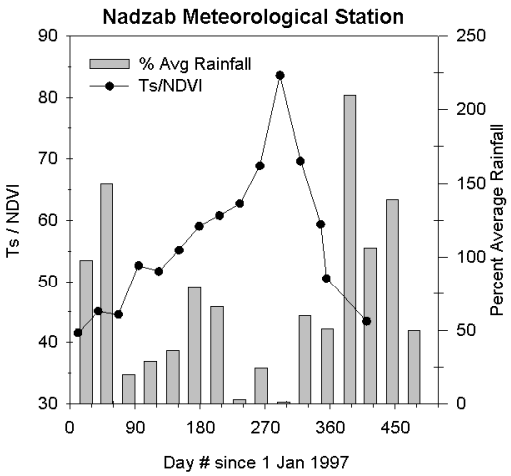

Fig. 22.2: Mean Ts/NDVI for the Nadzab region, derived from 4-week AVHRR composites, and percent average monthly rainfall for Nadzab since 1 Jan 1997.

7.0 Recommendations: Opportunities & Improvements

7.1 Opportunities

There are a number of opportunities which would allow full use of the composite AVHRR data for assessment and monitoring of the 1997 PNG drought situation. These are:

- Assessing the recovery phase of the drought during 1998 would be achieved by comparing the satellite data from 1998 with that recorded in 1996. UNDP have already committed funds for the project to purchase AVHRR composite data from CSIRO Marine Research in Hobart until the end of 1998. What is needed is the opportunity to allow analysts from PNG and Australia to work together to fully explore this.

- Working more closely with staff, with the appropriate technical skills (remote sensing and spatial information) and discipline training (agriculture), from PNG Department of Agriculture and Livestock would be of value. To date PNG_DATS has been installed in PNGGS, where they have ER-Mapper, the image processing system that the analysis is built around. It would be useful if PNG Department of Agriculture and Livestock also had ER-Mapper. Selected staff within the Department would require training for the package. An advantage of using ER-Mapper as the basis for PNG_DATS is that images do not need to be stored on disk after every processing option. Having "virtual datasets" greatly reduces the need for large hard disk space. Currently each of the 4-week composite images are 22 Megabytes (Mb) and over the three years there will be 39 base images in the time series. This totals 858 Mb of base data. If another image processing system was installed at PNG Department of Agriculture and Livestock then disk space would become an issue and large disks would be required.

- If would be beneficial to have access to a map, in digital format, of agricultural regions. Currently such exists with DAL, however due to a number of reasons including computer networking, we could access this for PNG_DATS which is currently located at PNGGS. If we could get access to this map this would allow analysis to be performed for only agricultural areas within each province. This level of detail would have been more useful to assess the drought situation for different agricultural production systems.

- A post-graduate degree candidate, possibly from within PNG Department of Agriculture, could fully establish the reasons for different responses within the context of the PNG 1997 drought. There is the opportunity to assess how to use remotely sensed data (which does not cover all of PNG area due to clouds) with generated surfaces of rainfall. It may be appropriate that this person be enrolled with ANU CRES and have contact with AGSO and CSIRO Land and Water staff.

Independent of the AVHRR time series data set developed here there are several opportunities that may in increase the understanding of drought in PNG. These are:

- Of direct relevance to developing a system for early prediction of drought in PNG Nicholls (1973) showed that weakened "Walker Circulation" sometimes corresponds to severe droughts in PNG. More recently, in Australia, rainfall (McBride and Nicholls, 1983, Nicholls, 1989) and crop yields of sorghum (Nicholls, 1986) and wheat (Rimmington and Nicholls, 1993) have been related to the El Niño Southern Oscillation (ENSO). ENSO can be thought of as a refinement of the weakened "Walker Circulation" introduced by (Nicholls, 1973). Examining historical trends of ENSO and drought occurrence in PNG may provide a drought early warning system. Some rules may be developed, possibly based on a combination of the magnitude, rate of change and the timing of the ENSO signal to indicate that PNG may soon experience drought conditions. When these hypothetical rules are met, it may be necessary to monitor both ground based meteorological data and hi-frequency remotely sensed data, as introduced in this report, to monitor development of the potential drought conditions. Ground based rainfall data can be in a root crop water balance model, with some probabilities of future rainfall amounts, to provide estimates of when crop failure may occur up to 8 weeks prior to the actual event (McApline *pers. comm*.). Southern Oscillation Index (SOI), which is based upon air pressure difference between Darwin and Tahiti provides a means of tracking changes in ENSO. SOI values can be obtained from the following WWW address:
  http://www.BoM.GOV.AU/climate/current/soihtm1.shtml

- In the Highlands, during the height of the drought, frost mapping could be attempted using night time thermal GMS data, which is recorded at hourly intervals. This could be combined with a DEM (to determine possible paths of cold air drainage) and maps of population distribution. This may show where drought affected the food supply to the subsistence based agricultural communities. This remote and synoptic study, would have to be validated by on ground field studies. Fig. 23 illustrates the type data visulation that can be performed when there is access to a DEM.

7.2 Recommended Future Improvements

Some improvements would have greatly helped in the establishment, transfer and analysis of PNG_DATS.

- At present the AVHRR composite period is 4-week. It would be preferable if the data was monthly (that is a composite period from the 1st of each month until the last day of the month). Monthly composites would allow easier transfer and extension to agricultural and relief staff. This may be accomplished by CSIRO Marine Research reprocessing the data to these periods. If that data is reprocessed, there is the opportunity to have digital data over the ocean parts of the image, not just the land. This may allow other applications to make use of this time series of AVHRR data.

- Access to ancillary digital data covering all of PNG would have been useful for the analysis within PNG_DATS. Possible sources of ancillary data could include PNGRIS, the digital elevation model (DEM) recently delivered to PNG DEC, and the improved vegetation polygons. The vegetation polygons required for this study would be based on a broad level of classification (not species or harvestable volumes) present in the PNG Forestry Authority Forest Information System (FIM). At the PNG Departmental level data custodian and transfer agreements are currently being addressed. Having an established protocol and point of contact for various data sets would have been extremely useful to this project.

8.0 Conclusions

Composite AVHRR imagery can be used to assess and monitor drought development and recovery in PNG. Cloud is a problem in PNG for reflective and thermal remotely sensed data, however, useful information was gained from this data set.

Transforming the AVHRR to the Ts/NDVI ratio provided a direct measure of environmental stress. This does not require ancillary meteorological data, and may be a useful data transformation to monitor drought conditions in other countries and regions. The Ts/NDVI ratio can be obtained from remotely sensed data alone. Not requiring ancillary ground based meteorological data may be an advantage for other countries.

9.0 Acknowledgments

This project was funded by the Papua New Guinea office of the United Nations Development Program (UNDP). Thanks are extended to all who willingly provided help and assistance in getting the project going in a short time frame. Paul Tildesley and Kim Badcock processed the AVHRR time series data base that was central to the project. Sam Maiha provided monthly rainfall data. AGSO SIMS staff (Ross Hill and Chris Fitzgerald) produced figures and the associated poster, CSIRO Land and Water staff (Heinz Buettikofer and Tony Tatarow) also produced some of the figures. Thanks are extended to all for wonderful graphics. Jim Mollison, ACRES, clarified RADAR data acquisition over PNG. Thanks to Drs

Bryant Allen, Mike Bourke, Alex Held, Gerry Jacobson, and John McAlpine for reviewing and making suggestions on an earlier draft that improved this final version.

10.0 References

Allen, B. (1989). Frost and Drought Through Time and Space, Part I: The Climatological Record. *Mountain Research and Development,* **9,** 252-278.

Allen, B., Brookfield, H. and Byron, Y. (1989). Frost and Drought Through Time and Space, Part II: The Written, Oral, and Proxy Records and their meaning. *Mountain Research and Development,* **9,** 252-278.

Allen, B.J. (1998). The 1997-98 Papua New Guinea Drought: Perceptions of Disaster. The Australian Centre for International and Tropical Health and Nutrition, University of Queensland, Brisbane, pp. 14.

Allen, B.J. and Bourke, R.M. (1997). Report of an Assessment of the Impacts of Frost and Drought in Papua New Guinea. Papua New Guinea Department of Provincial and Local Government Affairs, Canberra, pp. 20.

Allen, B.J., Bourke, R.M., Burton, J., Flew, S., Gaupu, B., Heia, S., Igua, P., Ivahupa, S., Kanua, M., Kokoa, P., Lillicrap, S., Ling, G., Lowe, M., Lutulele, R., Nongkas, A., Poienou, M., Risimeri, J., Sheldon, R., Sowei, J., Ukegawa, K., Willson, N., Wissink, D. and Woruba, M. (1997). Report of an Assessment of the Impacts of Frost and Drought in Papua New Guinea - Phase 2. Papua New Guinea Department of Provincial and Local Government Affairs, Canberra, pp. 27.

Alley, W.M. (1984). The Palmer Drought Severity Index: Limitations and Assumptions. *Journal of Climate and Applied Meteorology,* **23,** 1100-1109.

Alley, W.M. (1985). The Palmer Drought Severity Index as a Measure of Hydrologic Drought. *Water Resources Bulletin,* **21,** 105-114.

Bellamy, J.A. (1995). Landform Type. In *Papua New Guinea Inventory of Natural Resources, Population Distribution and Land Use Handbook*, Vol. 6 (Eds, Bellamy, J. A. and McAlpine, J. R.) AusAID, Canberra, pp. 162.

Bourke, R.M. (1988). Taim hangre: variation in subsistence food supply in the Papua New Guinea highlands. In *Department of Human Geography* Australian National University, Canberra.

Bourke, R.M. (1989). The Influence of Soil Moisture on Sweet Potato Yield in the Papua New Guinea Highlands. *Mountain Research and Development,* **9,** 322-321.

Bourke, R.M. (1998). Impact of the 1997 drought and frosts in Papua New Guinea. The Australian Centre for International and Tropical Health and Nutrition, University of Queensland, Brisbane, pp. 10.

Brookfield, H. and Allen, B. (1989). High-Altitude Occupation and Environment. *Mountain Research and Development,* **9,** 201-209.

Burgess, W. and Pairman, D. (1997). Bidirectional reflectance effects in NOAA AVHRR data. *International Journal of Remote Sensing,* **18,** 2815-2825.

Carlson, T.N., Gillies, R.R. and Perry, E.M. (1994). A method to make use of thermal infrared temperatures and NDVI measurements to infer soil water content and fractional vegetation cover. *Remote Sensing Reviews,* **9,** 161-173.

Carlson, T.N., Perry, E.M. and Schmugge, T.J. (1990). Remote Estimation of Soil Moisture Availability and Fractional Vegetation Cover for Agricultural Fields. *Agricultural and Forest Meteorology,* **52,** 45-69.

Choudhury, B.J. and DiGirolamo, N.E. (1995). Quantifying the Effect of Emissivity on the Relation between AVHRR Split Window Temperature Difference and Atmospheric Precipitable Water over Land Surface. *Remote Sensing of Environment,* **54,** 313-323.

Cognard, A.-L., Loumagne, C., Normand, M., Olivier, P., Ottle, C., Vidal-Madjar, D., Louahala, S. and Vidal, A. (1995). Evaluation of the ERS1 synthetic aperture radar capacity to estimate surface soil moisture: Two-year results over the Naizin watershed. *Water Resources Research,* **31,** 975-982.

Currey, B., Fraser, A.S. and Bardsley, K.L. (1987). How useful is Landsat monitoring? *Nature,* **328,** 587-589.

Deering, D.W. (1989). Field Measurements of Bidirectional Reflectance. In *Theory and Application of Optical Remote Sensing*(Ed, Asrar, G.) John Wiley and Sons, New York, pp. 14-65.

Gillies, R.R. and Carlson, T.N. (1995). Thermal remote sensing of surface soil water content with partial vegetation cover for incorporating into climate models. *Journal of Applied Meteorology,* **34,** 745-756.

Gillies, R.R., Carlson, T.N., Cui, J., Kustas, W.P. and Humes, K.S. (1997). A verification of the 'triangle' method for obtaining surface soil water content and energy fluxes from the remote measurements of the Normalized Difference Vegetation Index (NDVI) and surface radiant temperature. *International Journal of Remote Sensing,* **18,** 3145-3166.

Goetz, S.J. (1997). Multi-sensor analysis of NDVI, surface temperature and biophysical variables at a mixed grassland site. *International Journal of Remote Sensing,* **18,** 71-94.

Harrison, B.A. and Jupp, D.L.B. (1989). *Introduction to Remotely Sensed Data,* CSIRO Publications.

Held, A.A., Pidsley, D., Hatton, T.J. and Jupp, D.L.B. (1995). Use of Landsat TM data to scale measurements of evapotranspiration in the Northern Territory of Australia. In *Proceedings of the 2nd North Australian Remote Sensing and GIS forum* , Vol. AURISA Monograph No. 11 jointly by the Supervising Scientist and AURISA, Darwin, Australia, pp. 102-110.

Hobbs, T.J. (1997). Atmospheric correction of NOAA-11 NDVI data in the arid rangelands of Central Australia. *International Journal of Remote Sensing,* **18,** 1051-1058.

Hope, A.S. (1988). Estimation of wheat canopy resistance using combined remotely sensed spectral reflectance and thermal observations. *Remote Sensing of Environment,* **24,** 369-383.

Jupp, D.L.B., Tian, G., McVicar, T.R., Qin, Y. and Fuqin, L. (1998). Monitoring Soil Moisture Effects And Drought Using AVHRR Satellite Data I: Theory. CSIRO Earth Observation Centre, Canberra, pp. 89.

Kaufman, Y.J. and Tanre, D. (1992). Atmospherically Resistant Vegetation Index (ARVI) for EOS-MODIS. *IEEE Transactions on Geoscience and Remote Sensing,* **30,** 261-270.

Leprieur, C., Kerr, Y.H. and Pichon, J.M. (1996). Critical assessment of vegetation indices from AVHRR in a semi-arid environment. *International Journal of Remote Sensing,* **17,** 2549-2563.

McAlpine, J.R. (1995). Climate. In *Papua New Guinea Inventory of Natural Resources, Population Distribution and Land Use Handbook*, Vol. 6 (Eds, Bellamy, J. A. and McAlpine, J. R.) AusAID, Canberra, pp. 162.

McAlpine, J.R., Keig, G. and Falls, R. (1983). *Climate of Papua New Guinea,* ANU Press, Canberra.

McBride, J.L. and Nicholls, N. (1983). Seasonal relationships between Australian rainfall and the Southern Oscillation. *Monthly Weather Review,* **111,** 1998-2004.

McGwire, K. (1998). Improving Landsat Scene Selection Systems. *Photogrammetric Engineering and Remote Sensing,* **64,** 717-722.

McVicar, T.R. and Jupp, D.L.B. (1998). The current and potential operational uses of remote sensing to aid decisions on Drought Exceptional Circumstances in Australia: A Review. *Agricultural Systems,* **57,** 399- 468.

McVicar, T.R., Jupp, D.L.B., Yang, X. and Tian, G. (1992). Linking Regional Water Balance Models with Remote Sensing. In *Proceedings of the 13th Asian Conference on Remote Sensing* Ulaanbaatar, Mongolia, pp. B.6.1-B.6.6.

Moran, M.S., Clarke, T.R., Inoue, Y. and Vidal, A. (1994). Estimating crop water deficit using the relation between surface-air temperature and spectral vegetation index. *Remote Sensing of Environment,* **49,** 246-263.

Moran, M.S., Rahman, A.F., Washburne, J.C., Goodrich, D.C., Weltz, M.A. and Kustas, W.P. (1996). Combining the Penman-Monteith equation with measurements of surface temperature and reflectance to estimate evaporation rates of semiarid grassland. *Agriculture and Forest Meteorology,* **80,** 87-109.

Nemani, R.R., Pierce, L.L., Running, S.W. and Goward, S.N. (1993). Developing Satellite Derived Estimates of Surface Moisture Status. *Journal of Applied Meteorology,* **32,** 548-557.

Nemani, R.R. and Running, S.W. (1989). Estimation of Regional Surface Resistance to Evapotranspiration from NDVI and Thermal-IR AVHRR Data. *Journal of Applied Meteorolgy,* **28,** 276-284.

Nicholls, N. (1973). The Walker Circulation and Papua New Guinea Rainfall. Australian Bureau of Meterology, , pp. 13.

Nicholls, N. (1986). Use of Southern Oscillation to predict Australian sorghum yield. *Agricultural and Forest Meteorology,* **38,** 9-15.

Nicholls, N. (1989). Sea surface temperature and Australian winter rainfall. *Journal of Climate,* **2,** 965-973.

Petty, G.W. (1995). The Status of Satellite-Based Rainfall Estimation Over Land. *Remote Sensing of Environment,* **51,** 125-137.

Prata, A.J. (1994). Land Surface Temperature. In *AVHRR Workshop Proceedings, 28 February* , Vol. 67-78 (Ed, Prata, A. J.) CSIRO Division of Atmospheric Research, Melbourne, Australia.

Prata, A.J., Caselles, V., Coll, C., Ottle, C. and Sobrino, J. (1995). Thermal remote sensing of land surface temperature from satellites: Current status and future prospects. *Remote Sensing Reviews,* **12,** 175-224.

Price, J.C. (1990). Using Spatial Context in Satellite Data to Infer Regional Scale Evapotranspiration. *IEEE Transactions on Geoscience and Remote Sensing,* **GE-28,** 940-948.

Rimmington, G.M. and Nicholls, N. (1993). Forecasting Wheat Yields in Australia with the Southern Oscillation Index. *Austustralian Journal of Agricultural Research,* **44,** 625-632.

Saunders, R.R. and Kriebel, K.T. (1988). An Improved method for detecting clear sky and cloudy radiances from AVHRR data. *International Journal of Remote Sensing,* **9,** 123-150.

Sellers, P.J. (1985). Canopy reflectance, photosynthesis and transpiration. *International Journal of Remote Sensing,* **6,** 1335-1372.

Sellers, P.J. (1987). Canopy reflectance, photosynthesis and transpiration. II. The role of biophysics in the linearity of their interdependence. *Remote Sensing of Environment,* **21,** 143-183.

Thenkabail, P.S., Ward, A.B., Lyon, J.G. and Merry, C.J. (1994). Thematic Mapper vegetation indices for determining soybean and corn growth parameters. *Photogrammetric Engineering and Remote Sensing,* **60,** 437-442.

Tian, G. (1989). Spectral Signatures and Vegetation Indices of Crops. CSIRO Division of Water Resources, Canberra, ACT, .

Tucker, C.J. (1979). Red and photographic infrared linear combinations for monitoring vegetation. *Remote Sensing of Environment,* **8,** 127-150.

White, D.H. (1990). A Study of the Feasibility of Using Simulation Models and Mathematical Programs as Aids to Drought Monitoring and Management. Bureau of Rural Resources, Canberra, .

Wilhite, D.A. (Ed.) (1993). *Drought Assessment, Management, and Planning: Theory and Case Studies,* Kluwer Academic Publishers, Boston.

Wilhite, D.A. and Glantz, M.H. (1985). Understanding the drought phenomenon: The role of definitions. *Water International,* **10,** 111-120.

WMO (1975). Droughts and Agriculture. World Meteorological Organization, .

Yang, X., Zhou, Q. and Melville, M. (1997). Estimating local sugarcane evapotranspiration using LANDSAT TM image and a VITT concept. *International Journal of Remote Sensing,* **18,** 453-459.

11.0 Appendix 1 Organisations and Individuals Consulted.

Australian Geological Survey Organisation	Gerry Jacobson	61-2-6249-9758
Australian National University - Deptartment of Human Geography	Bryant Allen	61-2-6249-4347
	Mike Bourke	61-2-6249-4345
	Janine Conway	61-2-6249-2246
	Robin Grau	61-2-6249-3830
	Luke Hanson	61-2-6249-4344
Australian National University - Centre for Resource and Environmental Studies	Michael Hutchinson	61-2-6249-4783
	Henry Nix	61-2-6249-4588
	Mike Hedermark	675-325-4900
Bureau of Meteorology Research Centre	Neville Nicholls	61-3-9669-4407
CSIRO Land and Water	Alex Held	61-2-6246-5718
CSIRO Marine Research	Kim Badock	61-3-6232-5398
	Paul Tildesley	61-3-6232-5251
Private Consultant	John McAlpine	61-7-3371-3989
PNG Agriculture and Livestock	Balthazar Wayi	675-320-0658
	Michael Siri	675-321-4458
	Francias Diank	675-321-4458
	Regina Kiele	675-321-4458
	Joseph Silki	675-321-4673
PNG Environment and Conservation	Kembi Watoki	675-301-1607
PNG Forestry Authority	Martin Golman	675-327-7874
PNG Geological Survey	Joe Buleka	675-325-4424
	Elizabeth Michael	675-325-4425
	Gabriel Kuna	675-325-4425
PNG National Mapping Bureau	David Freyne	675-327-6529
PNG National Weather Service	Sam Maiha	675-325-2788
United Nations Development Program	Benard Choulai	675-321-2877
	Finn Reske-Nielsen	675-321-2877
	Peter Witham	675-321-2877

12.0 Appendix 2: Listing of look-up-tables (LUT)

These LUT are used to convert between digital number and physical units for 5 of the 11 channels of the CSIRO Marine Research composite AVHRR images.

	Chn_1	Chn_2	Chn_9	Chn_10	Chn_11
Digital Number	Albedo Channel 1 (%)	Albedo Channel 2 (%)	BT3-BT4 (°C)	BT4 (°C)	BT4-BT5 (°C)
0	0	0	-2	< -63.5	-2.95
1	0	0	-2	-63.25	-2.9
2	0.1	0.1	-1.9	-62.75	-2.79
3	0.2	0.2	-1.8	-62.25	-2.67
4	0.3	0.3	-1.7	-61.75	-2.57
5	0.41	0.41	-1.6	-61.25	-2.46
6	0.51	0.51	-1.49	-60.75	-2.36
7	0.61	0.61	-1.39	-60.25	-2.27
8	0.72	0.72	-1.29	-59.75	-2.17
9	0.83	0.83	-1.18	-59.25	-2.08
10	0.93	0.93	-1.08	-58.75	-1.99
11	1.04	1.04	-0.97	-58.25	-1.91
12	1.15	1.15	-0.87	-57.75	-1.82
13	1.26	1.26	-0.76	-57.25	-1.74
14	1.37	1.37	-0.66	-56.75	-1.66
15	1.48	1.48	-0.55	-56.25	-1.59
16	1.59	1.59	-0.44	-55.75	-1.51
17	1.71	1.71	-0.33	-55.25	-1.44
18	1.82	1.82	-0.23	-54.75	-1.37
19	1.94	1.94	-0.12	-54.25	-1.31
20	2.05	2.05	-0.01	-53.75	-1.24
21	2.17	2.17	0.1	-53.25	-1.18
22	2.29	2.29	0.21	-52.75	-1.12
23	2.41	2.41	0.33	-52.25	-1.06
24	2.53	2.53	0.44	-51.75	-1
25	2.65	2.65	0.55	-51.25	-0.95
26	2.77	2.77	0.66	-50.75	-0.89
27	2.89	2.89	0.78	-50.25	-0.84
28	3.01	3.01	0.89	-49.75	-0.79
29	3.14	3.14	1.01	-49.25	-0.74
30	3.26	3.26	1.12	-48.75	-0.69
31	3.39	3.39	1.24	-48.25	-0.65
32	3.52	3.52	1.35	-47.75	-0.6
33	3.65	3.65	1.47	-47.25	-0.56
34	3.78	3.78	1.59	-46.75	-0.52
35	3.91	3.91	1.71	-46.25	-0.48
36	4.04	4.04	1.82	-45.75	-0.44
37	4.17	4.17	1.94	-45.25	-0.4
38	4.31	4.31	2.06	-44.75	-0.36
39	4.44	4.44	2.18	-44.25	-0.33
40	4.58	4.58	2.31	-43.75	-0.29
41	4.71	4.71	2.43	-43.25	-0.26
42	4.85	4.85	2.55	-42.75	-0.23
43	4.99	4.99	2.67	-42.25	-0.2
44	5.13	5.13	2.8	-41.75	-0.17

45	5.27	5.27	2.92	-41.25	-0.14
46	5.42	5.42	3.05	-40.75	-0.11
47	5.56	5.56	3.17	-40.25	-0.08
48	5.71	5.71	3.3	-39.75	-0.05
49	5.85	5.85	3.42	-39.25	-0.03
50	6	6	3.55	-38.75	0
51	6.15	6.15	3.68	-38.25	0.03
52	6.3	6.3	3.81	-37.75	0.05
53	6.45	6.45	3.94	-37.25	0.08
54	6.6	6.6	4.07	-36.75	0.1
55	6.75	6.75	4.2	-36.25	0.13
56	6.91	6.91	4.33	-35.75	0.15
57	7.06	7.06	4.46	-35.25	0.18
58	7.22	7.22	4.6	-34.75	0.21
59	7.38	7.38	4.73	-34.25	0.23
60	7.54	7.54	4.86	-33.75	0.26
61	7.7	7.7	5	-33.25	0.28
62	7.86	7.86	5.13	-32.75	0.31
63	8.03	8.03	5.27	-32.25	0.34
64	8.19	8.19	5.41	-31.75	0.37
65	8.36	8.36	5.54	-31.25	0.39
66	8.53	8.53	5.68	-30.75	0.42
67	8.69	8.69	5.82	-30.25	0.45
68	8.86	8.86	5.96	-29.75	0.48
69	9.04	9.04	6.1	-29.25	0.5
70	9.21	9.21	6.24	-28.75	0.53
71	9.38	9.38	6.38	-28.25	0.56
72	9.56	9.56	6.52	-27.75	0.59
73	9.74	9.74	6.67	-27.25	0.62
74	9.91	9.91	6.81	-26.75	0.65
75	10.1	10.1	6.95	-26.25	0.68
76	10.28	10.28	7.1	-25.75	0.71
77	10.46	10.46	7.25	-25.25	0.74
78	10.64	10.64	7.39	-24.75	0.77
79	10.83	10.83	7.54	-24.25	0.79
80	11.02	11.02	7.69	-23.75	0.82
81	11.21	11.21	7.84	-23.25	0.86
82	11.4	11.4	7.99	-22.75	0.89
83	11.59	11.59	8.14	-22.25	0.92
84	11.78	11.78	8.29	-21.75	0.95
85	11.98	11.98	8.44	-21.25	0.98
86	12.17	12.17	8.59	-20.75	1.01
87	12.37	12.37	8.75	-20.25	1.04
88	12.57	12.57	8.9	-19.75	1.07
89	12.77	12.77	9.05	-19.25	1.1
90	12.98	12.98	9.21	-18.75	1.14
91	13.18	13.18	9.37	-18.25	1.17
92	13.39	13.39	9.52	-17.75	1.2
93	13.59	13.59	9.68	-17.25	1.23
94	13.8	13.8	9.84	-16.75	1.27
95	14.02	14.02	10	-16.25	1.3
96	14.23	14.23	10.16	-15.75	1.33
97	14.44	14.44	10.32	-15.25	1.37
98	14.66	14.66	10.48	-14.75	1.4
99	14.88	14.88	10.65	-14.25	1.43
100	15.1	15.1	10.81	-13.75	1.47
101	15.32	15.32	10.97	-13.25	1.5
102	15.54	15.54	11.14	-12.75	1.54

103	15.77	15.77	11.31	-12.25	1.57
104	16	16	11.47	-11.75	1.61
105	16.22	16.22	11.64	-11.25	1.64
106	16.45	16.45	11.81	-10.75	1.68
107	16.69	16.69	11.98	-10.25	1.71
108	16.92	16.92	12.15	-9.75	1.75
109	17.16	17.16	12.32	-9.25	1.78
110	17.4	17.4	12.49	-8.75	1.82
111	17.64	17.64	12.67	-8.25	1.86
112	17.88	17.88	12.84	-7.75	1.89
113	18.12	18.12	13.01	-7.25	1.93
114	18.37	18.37	13.19	-6.75	1.97
115	18.62	18.62	13.37	-6.25	2
116	18.87	18.87	13.54	-5.75	2.04
117	19.12	19.12	13.72	-5.25	2.08
118	19.37	19.37	13.9	-4.75	2.12
119	19.63	19.63	14.08	-4.25	2.16
120	19.89	19.89	14.26	-3.75	2.2
121	20.15	20.15	14.44	-3.25	2.23
122	20.41	20.41	14.63	-2.75	2.27
123	20.67	20.67	14.81	-2.25	2.31
124	20.94	20.94	14.99	-1.75	2.35
125	21.21	21.21	15.18	-1.25	2.39
126	21.48	21.48	15.36	-0.75	2.43
127	21.75	21.75	15.55	-0.25	2.47
128	22.03	22.03	15.74	0.25	2.51
129	22.3	22.3	15.93	0.75	2.55
130	22.58	22.58	16.12	1.25	2.59
131	22.87	22.87	16.31	1.75	2.64
132	23.15	23.15	16.5	2.25	2.68
133	23.44	23.44	16.7	2.75	2.72
134	23.72	23.72	16.89	3.25	2.76
135	24.02	24.02	17.08	3.75	2.8
136	24.31	24.31	17.28	4.25	2.85
137	24.6	24.6	17.48	4.75	2.89
138	24.9	24.9	17.68	5.25	2.93
139	25.2	25.2	17.87	5.75	2.98
140	25.51	25.51	18.07	6.25	3.02
141	25.81	25.81	18.28	6.75	3.06
142	26.12	26.12	18.48	7.25	3.11
143	26.43	26.43	18.68	7.75	3.15
144	26.74	26.74	18.88	8.25	3.2
145	27.06	27.06	19.09	8.75	3.24
146	27.37	27.37	19.29	9.25	3.29
147	27.69	27.69	19.5	9.75	3.33
148	28.02	28.02	19.71	10.25	3.38
149	28.34	28.34	19.92	10.75	3.43
150	28.67	28.67	20.13	11.25	3.47
151	29	29	20.34	11.75	3.52
152	29.33	29.33	20.55	12.25	3.57
153	29.67	29.67	20.77	12.75	3.61
154	30.01	30.01	20.98	13.25	3.66
155	30.35	30.35	21.2	13.75	3.71
156	30.7	30.7	21.41	14.25	3.76
157	31.04	31.04	21.63	14.75	3.81
158	31.39	31.39	21.85	15.25	3.86
159	31.74	31.74	22.07	15.75	3.91
160	32.1	32.1	22.29	16.25	3.95

161	32.46	32.46	22.51	16.75	4
162	32.82	32.82	22.73	17.25	4.05
163	33.18	33.18	22.96	17.75	4.11
164	33.55	33.55	23.18	18.25	4.16
165	33.92	33.92	23.41	18.75	4.21
166	34.29	34.29	23.64	19.25	4.26
167	34.67	34.67	23.87	19.75	4.31
168	35.05	35.05	24.1	20.25	4.36
169	35.43	35.43	24.33	20.75	4.42
170	35.81	35.81	24.56	21.25	4.47
171	36.2	36.2	24.79	21.75	4.52
172	36.59	36.59	25.03	22.25	4.57
173	36.99	36.99	25.26	22.75	4.63
174	37.39	37.39	25.5	23.25	4.68
175	37.79	37.79	25.74	23.75	4.74
176	38.19	38.19	25.98	24.25	4.79
177	38.6	38.6	26.22	24.75	4.85
178	39.01	39.01	26.46	25.25	4.9
179	39.42	39.42	26.7	25.75	4.96
180	39.84	39.84	26.95	26.25	5.01
181	40.26	40.26	27.19	26.75	5.07
182	40.68	40.68	27.44	27.25	5.13
183	41.11	41.11	27.69	27.75	5.18
184	41.54	41.54	27.94	28.25	5.24
185	41.97	41.97	28.19	28.75	5.3
186	42.41	42.41	28.44	29.25	5.36
187	42.85	42.85	28.69	29.75	5.42
188	43.3	43.3	28.94	30.25	5.48
189	43.75	43.75	29.2	30.75	5.54
190	44.2	44.2	29.46	31.25	5.6
191	44.65	44.65	29.71	31.75	5.66
192	45.11	45.11	29.97	32.25	5.72
193	45.57	45.57	30.23	32.75	5.78
194	46.04	46.04	30.5	33.25	5.84
195	46.51	46.51	30.76	33.75	5.9
196	46.99	46.99	31.02	34.25	5.96
197	47.46	47.46	31.29	34.75	6.02
198	47.94	47.94	31.56	35.25	6.09
199	48.43	48.43	31.82	35.75	6.15
200	48.92	48.92	32.09	36.25	6.21
201	49.41	49.41	32.37	36.75	6.28
202	49.91	49.91	32.64	37.25	6.34
203	50.41	50.41	32.91	37.75	6.41
204	50.92	50.92	33.19	38.25	6.47
205	51.43	51.43	33.46	38.75	6.54
206	51.94	51.94	33.74	39.25	6.6
207	52.46	52.46	34.02	39.75	6.67
208	52.98	52.98	34.3	40.25	6.74
209	53.5	53.5	34.58	40.75	6.81
210	54.04	54.04	34.87	41.25	6.87
211	54.57	54.57	35.15	41.75	6.94
212	55.11	55.11	35.44	42.25	7.01
213	55.65	55.65	35.73	42.75	7.08
214	56.2	56.2	36.02	43.25	7.15
215	56.75	56.75	36.31	43.75	7.22
216	57.31	57.31	36.6	44.25	7.29
217	57.87	57.87	36.89	44.75	7.36
218	58.43	58.43	37.19	45.25	7.43

219	59	59	37.49	45.75	7.5
220	59.58	59.58	37.78	46.25	7.57
221	60.16	60.16	38.08	46.75	7.65
222	60.74	60.74	38.38	47.25	7.72
223	61.33	61.33	38.69	47.75	7.79
224	61.92	61.92	38.99	48.25	7.87
225	62.52	62.52	39.3	48.75	7.94
226	63.12	63.12	39.6	49.25	8.02
227	63.73	63.73	39.91	49.75	8.09
228	64.34	64.34	40.22	50.25	8.17
229	64.96	64.96	40.54	50.75	8.24
230	65.58	65.58	40.85	51.25	8.32
231	66.21	66.21	41.16	51.75	8.4
232	66.84	66.84	41.48	52.25	8.48
233	67.48	67.48	41.8	52.75	8.55
234	68.12	68.12	42.12	53.25	8.63
235	68.77	68.77	42.44	53.75	8.71
236	69.42	69.42	42.76	54.25	8.79
237	70.08	70.08	43.09	54.75	8.87
238	70.74	70.74	43.41	55.25	8.95
239	71.41	71.41	43.74	55.75	9.03
240	72.08	72.08	44.07	56.25	9.12
241	72.76	72.76	44.4	56.75	9.2
242	73.45	73.45	44.74	57.25	9.28
243	74.14	74.14	45.07	57.75	9.36
244	74.83	74.83	45.41	58.25	9.45
245	75.53	75.53	45.74	58.75	9.53
246	76.24	76.24	46.08	59.25	9.62
247	76.95	76.95	46.42	59.75	9.7
248	77.67	77.67	46.77	60.25	9.79
249	78.4	78.4	47.11	60.75	9.87
250	79.13	79.13	47.46	61.25	9.96
251	79.86	79.86	47.81	61.75	10.05
252	80.61	80.61	48.16	62.25	10.14
253	81.35	81.35	48.51	62.75	10.23
254	82.11	82.11	48.86	63.25	10.28
255	null	null	null	null	null